Cell Communication and Signaling

RESEARCH

Open Access

Exosomes derived from IFNγ-stimulated mesenchymal stem cells protect photoreceptors in RCS rats by restoring immune homeostasis through tsRNAs

Luodan A[1,2†], Linghui Qu[2,3†], Juncai He[1,2], Lingling Ge[1,2], Hui Gao[1,2,4], Xiaona Huang[1,2], Tianjing You[1,2], Hong Gong[2,5], Qingle Liang[6], Siyu Chen[1,2], Jing Xie[1,2*] and Haiwei Xu[1,2*]

Abstract

Background Retinitis pigmentosa is a neurodegenerative disease with major pathologies of photoreceptor apoptosis and immune imbalance. Mesenchymal stem cells (MSCs) have been approved for clinical application for treating various immune-related or neurodegenerative diseases. The objective of this research was to investigate the mechanisms underlying the safeguarding effects of MSC-derived exosomes in a retinal degenerative disease model.

Methods Interferon gamma-stimulated exosomes (IFNγ-Exos) secreted from MSCs were isolated, purified, and injected into the vitreous body of RCS rats on postnatal day (P) 21. Morphological and functional changes in the retina were examined at P28, P35, P42, and P49 in Royal College of Surgeons (RCS) rats. The mechanism was explored using high-throughput sequencing technology and confirmed in vitro.

Results Treatment with IFNγ-Exo produced better protective effects on photoreceptors and improved visual function in RCS rats. IFNγ-Exo significantly suppressed the activated microglia and inhibited the inflammatory responses in the retina of RCS rats, which was also confirmed in the lipopolysaccharide-activated microglia cell line BV2. Furthermore, through tRNA-derived small RNA (tsRNA) sequencing, we found that IFNγ-Exos from MSCs contained higher levels of Other-1_17-tRNA-Phe-GAA-1-M3, Other-6_23-tRNA-Lys-TTT-3, and TRF-57:75-GLN-CGG-2-m2 than native exosomes, which mainly regulated inflammatory and immune-related pathways, including the mTOR signaling pathway and EGFR tyrosine kinase inhibitor resistance.

Conclusions IFNγ stimulation enhanced the neuroprotective effects of MSC-derived exosomes on photoreceptors of the degenerative retina, which may be mediated by immune regulatory tsRNAs acting on microglia. In conclusion, IFNγ-Exo is a promising nanotherapeutic agent for the treatment of retinitis pigmentosa.

Keywords Exosomes, Retinitis pigmentosa, Mesenchymal stem cells, Inflammatory regulation, Immunomodulation

†Luodan A and Linghui Qu contributed equally to this work.

*Correspondence:
Jing Xie
xiejingrain@163.com
Haiwei Xu
xuhaiwei@tmmu.edu.cn
Full list of author information is available at the end of the article

Graphical Abstract

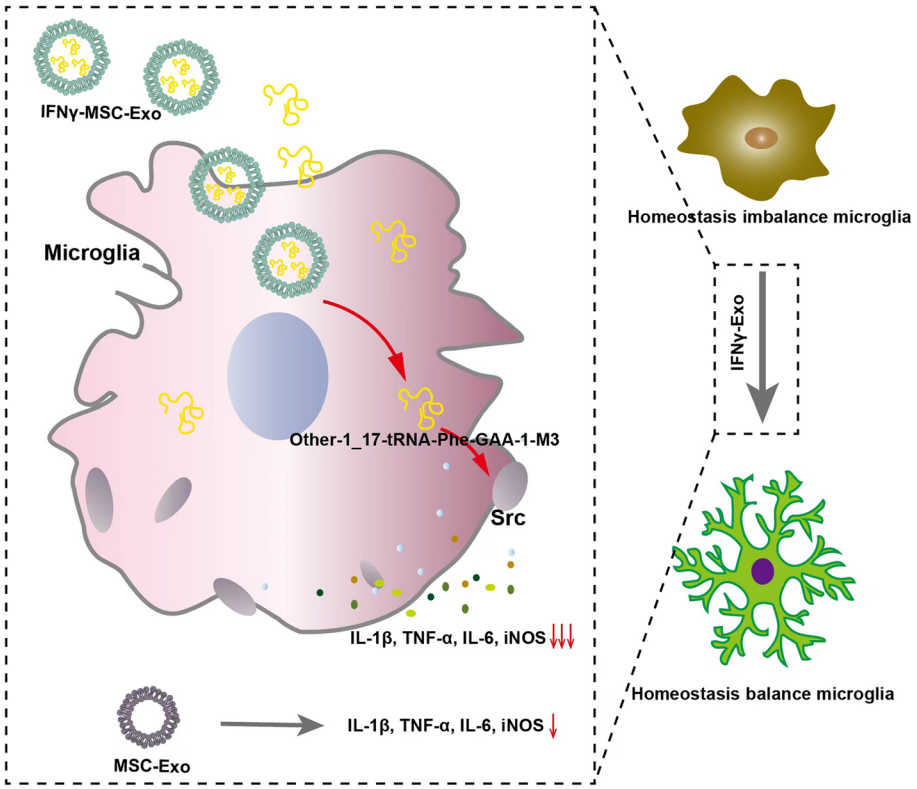

Introduction

Retinitis pigmentosa (RP) induces irreversible vision loss, with key pathological changes including photoreceptor apoptosis and immune imbalance. Although there is still no effective treatment for RP, immunomodulatory therapy has been regarded as a promising approach in clinical applications to protect the retina and slow photoreceptor degeneration [1].

Mesenchymal stem cells (MSCs) have demonstrated excellent therapeutic effects on various neurodegenerative diseases because of their unique multi-differentiation potential and potent immune regulation capabilities [2–5]. The therapeutic effects of MSCs and their interaction with the immune system appear to mainly occur through the paracrine pathway [6], through the secretion of soluble factors, including growth factors, cytokines, chemokines, and extracellular vesicles (EVs) [7, 8]. EVs comprise two general sizes, larger vesicles > 200 nm in diameter and smaller vesicles, i.e., exosomes, with a diameter between 30 and 200 nm. Exosomes, which are lipid bilayer vesicles, are actively discharged by mammalian cells, including MSCs, contributing to intercellular communication [9, 10].

As a cell-free therapy, MSC-derived exosomes (MSC-Exos) have been used in a series of neurodegenerative diseases and have shown significant functional improvement. Indeed, exosomes derived from bone marrow mesenchymal cells (BMSCs) have been shown to significantly improve the behavior of experimental autoimmune encephalomyelitis (EAE) rats by promoting the polarization of microglia from M1 to M2 and secreting anti-inflammatory cytokines [11]. Moreover, in experimental autoimmune uveoretinitis (EAU) mice, treatment with MSC-Exos significantly rescued damaged photoreceptors and retinal infiltration of $CD3^+$ T cells and macrophages [12, 13]. A similar improvement in visual function has been found in a rat retinal ischemia model with the infusion of MSC-Exos into the vitreous humor, through reduction of neuroinflammation and apoptosis [14]. It has also been shown that MSC-Exos enhances hippocampal neurogenesis and improves memory in Alzheimer's disease mice through the suppression of over-activated microglial cells and astrocytes [15]. These

results demonstrate that MSC-Exos produce neuroprotection partially through their specific immune regulation in the nervous system.

The characteristics of exosomes vary greatly among different cell types or subpopulations from which they are secreted. External stimuli during MSC culture can change the cargoes of exosomes, and preconditioning MSCs with specific stimuli can improve the ratio and purity of exosomes with specific therapeutic effects. Indeed, pretreatment of MSCs with certain cytokines, chemicals, or hypoxia has been proven to improve their immunomodulatory and regenerative effects [16]. A recent study showed that intraocular injection of TNF-α-stimulated gingival MSC exosomes markedly suppressed inflammation and produced better protective effects on the retinal cells of retinal ischemia-reperfusion injury (IRI) mice than native exosomes [17]. Moreover, exosomes derived from human MSCs stimulated by IFNγ have been shown to produce better therapeutic effects than native exosomes in EAE mice [18], although the underlying mechanisms have not been clarified. As a typical inherited retinal degenerative (RD) disease, RP is characterized by the loss of photoreceptor and/or retinal pigment epithelial (RPE) cells, leading to the deterioration of the retinal immune microenvironment and ultimately causing vision loss [19, 20]. Our previous study demonstrated that exosomes derived from neural stem cells were engulfed by activated microglia in the retina of Royal College of Surgeons (RCS) rats and delayed retinal degeneration by specifically suppressing microglial overactivation [21].

Low production is a major challenge in the clinical application of exosomes. A series of strategies have been used to improve the production of exosomes including physical, chemical, and biological stimulation to the cells [22]. The physical stimulation, including mechanical load, geometric, acoustic, and electrical. Among these, the mechanical load was proved to significantly increase the exosome production, as high as 150 times higher than the traditional methods of cultivation [23]. Chemical stimulation is another effective strategy to increase exosome production by adding chemical compounds including oxidative phosphorylation and glycolysis inhibitors, inhibitors of end lysosomal transport, adiponectin, small molecule modulators including n-methyl dopamine, and norepinephrine [22]. Manipulation of key genes involved in exosome biogenesis and recycling including heat shock protein, TSPAN 6, systemin, FYVE-type zinc finger (PIKfyve), ISGylation, and Corneum was reported recently [24]. Regulating environmental stimuli, such as hypoxia, pondus hydrogenii (PH), and glucose content, among which PH is a more promising environmental stimulus was used to improve the production of exosomes [25]. However, studies of environmental factors are mostly concerned with the nature of exosomes rather than the amount of secretion [22, 24]. Based on the therapeutic effect of MSC-derived exosomes in RP [26], we aimed to optimize the therapeutic effect and explore the mechanism of stem cell therapy and new cell-free therapy. Therefore, when we choose the way to optimize exosomes, we should consider not only the yield, but also the performance. Exosome production and active loading of contents are related to external stimuli, the most important and convenient of which is to pretreat the exosome-producing cells with cytokines (e.g. IFN-γ, IL-1β, TNF-α, TGF-β). Among them, activation of MSCs by IFNγ enhances the immunosuppressive ability of MSC-derived exosomes, and more importantly, enhances their anti-inflammatory ability and therapeutic efficacy in a variety of immune-related diseases and neurodegenerative diseases [27–33]. However, the mechanism by which IFNγ regulates the immunomodulatory and inflammatory inhibition capacity of exosomes produced by MSCs is unclear, and that has not been reported in RP. Therefore, this study was devoted to studying the changes in exosomes after IFNγ pretreatment and its effect on retinitis pigmentosa.

The effects of exosomes are determined by their cargoes, including proteins, mRNAs, and non-coding RNAs (ncRNAs). As documented in numerous studies, various ncRNAs, mainly miRNAs and lncRNAs, are present in abundant quantities within exosomes and engage with recipient cells to regulate cellular functions and the progression of diseases. Additionally, recent research indicates that tsRNAs, a subtype of ncRNAs, are also widely found in exosomes, exhibiting enhanced stability [34]. tRFs and tiRNAs can be transferred to recipient cells via exosomes to play a role [35, 36]. In addition, as one of the non-coding small RNAs in exosomes, tsRNA has several advantages. The proportion of different types of tsRNAs might be used as a marker of disease diagnosis [37, 38]. Compared with miRNA, tsRNA is more stable and has conservation between species [39]. Meanwhile, tsRNAs can regulate gene expression in more ways than that in miRNAs [40]. In addition, tsRNA contains abundant modifications, which is closely related to the richness of its functions [41], so tsRNAs are being considered as potential biomarkers for detection and as minimally invasive therapeutic tools [42]. It has shown that BMSC-derived exosomes loaded with tsRNA-10,277 enhance the osteogenic differentiation ability of BMSCs, which is of great significance for the treatment of osteonecrosis of the femoral head [43]. Despite this, the specific role of exosomal tsRNAs remains poorly understood, particularly within the context of neurodegenerative diseases. The structure of tsRNAs, generally comprising only

14–40 specific nucleotides, is stable and highly conservative. tsRNAs have been roughly divided into two categories: tRNA-derived fragments (tRFs), which are generated by mature or precursor sequences of tRNA, and tRNA-derived stress-induced RNA (tiRNA), which are generated by cutting mature tRNA sequences at the anti-codon position [44, 45]. Multiple studies have shown that tRFs and tiRNAs are biologically active in the regulation of gene expression and translation [46, 47], epigenetic regulation [48], and intercellular communication [49], among others. tsRNAs are involved in regulation and are pivotal to the development of neurodegenerative diseases, immune-related diseases, tumors, and metabolic diseases [35, 39]. It has been demonstrated that tsRNA-21,109 in MSC-Exos inhibits the M1-type polarization of macrophages, thereby delaying systemic lupus erythematosus [50]. Recently, it was shown that the expression of tRFs and tiRNAs in exosomes was affected by the immune microenvironment [51]. However, it remains unclear whether the IFNγ level in the microenvironment affects the expression of tRFs and tiRNAs in the exosomes of MSCs and their effects on retina degeneration.

In the present study, we sequenced the tRF and tiRNA expression profiles of MSC-derived exosomes and analyzed the influence of IFNγ stimulation, as well as the effects of MSC-Exos on the development of retinal degeneration. Our results demonstrated that IFNγ stimulation enhanced the neuroprotection of MSCs-Exos and delayed retinal degeneration partially through suppression of microglial overactivation and retinal inflammation via tsRNA-mediated down-modulation of Src expression.

Results

Characteristics of IFNγ-Exos extracted from bone marrow MSCs

MSCs were isolated from the femur and tibia of wild-type rats and purified by subculture. The MSCs showed uniform and clear contours with a long spindle shape (Supplementary Material, Figure S1A). Flow cytometry confirmed that more than 90% of MSCs expressed CD29, CD90, CD105, and CD44, whereas only 1% expressed CD11b, CD34, and CD45 (Figure S1B). Moreover, the MSCs demonstrated spontaneous osteogenic, adipogenic, and chondrogenic differentiation potential, as shown in Figure S1C–E.

To analyze the influence of IFNγ stimulation on the characteristics of exosomes, rat MSCs were evenly divided into two groups. The exosomes were extracted separately from the conditional medium in which MSCs had been cultured for 48 h with or without 50 ng/mL IFNγ stimulation; that is, with either IFNγ-stimulated exosomes (IFNγ-Exos) or native exosomes (Native-Exos), respectively (Fig. 1A). Transmission electron microscopy (TEM) images confirmed that the exosomes exhibited a spherical shape (Fig. 1B). Nanoparticle tracking analysis (NTA) revealed that the exosomes had an average diameter of approximately 115 nm in the Native-Exo group and 119 nm in the IFNγ-Exo group (Fig. 1C). The overall exosome concentration in the IFNγ-Exo group was higher than that in the Native-Exo group (Fig. 1D). Upon analysis, it was observed that the IFNγ-Exo group had a lower count of exosomes with a particle size ranging from 50 to 100 nm compared to the Native-Exo group. Conversely, the IFNγ group exhibited a higher count of exosomes with a larger particle size of 150–200 nm when compared to the Native-Exo group (Fig. 1E). Western blotting (WB) further confirmed that exosomes in both groups expressed exosomal signature proteins, including CD63, CD81, and CD9 (Fig. 1F). Notably, IFNγ treatment upregulated the expression of CD63, CD81, and CD9 proteins (Fig. 1G-I).

To exclude the possibility that the increase in exosomes in the IFNγ-Exo group was caused by the increased proliferation of MSCs, the morphology of MSCs (Figure S2A), CCK-8 cell activity analysis (Figure S2B), and flow cytometry apoptosis detection (Figure S2C, D) were performed. These results demonstrate that IFNγ not significantly influences the viability or apoptosis of MSCs, suggesting that IFNγ promotes MSCs to produce more exosomes with larger diameters.

IFNγ-Exos improves the visual function of RCS rats

To assess the therapeutic effect of different exosomes, we injected equal amounts of IFNγ-Exos and Native-Exos (1×10^{11}/eye) into the vitreous cavity of RCS rats on 21

(See figure on next page.)

Fig. 1 Characteristics of exosomes isolated from rat MSCs and the influences of IFNγ pretreatment. **A** Procedure diagram of the exosomes obtained. **B**, **B$_1$** Typical morphology of exosomes under TEM ($n=3$). **C**, **C$_1$** Typical NTA curves and image display of exosomes in the Native-Exo and IFNγ-Exo groups. **D** The relative number of exosomes in the two groups was analyzed by NTA ($n=12$). **E** NTA was used to analyze the proportion of exosomes of the Native-Exo and IFNγ-Exo groups in different particle size distribution ranges ($n=12$). **F** Representative images of western blot showing exosomal protein markers (CD63, CD81, CD9) in the Native-Exo and IFNγ-Exo groups. **G–I** Comparison of protein grayscale analysis of CD63, CD81, and CD9 between the Native-Exo and IFNγ-Exo groups ($n=6$). Data represent the mean ± SEM.* $P<0.05$, *** $P<0.001$, **** $P<0.0001$. Scale bars: 200 μm, 20 μm

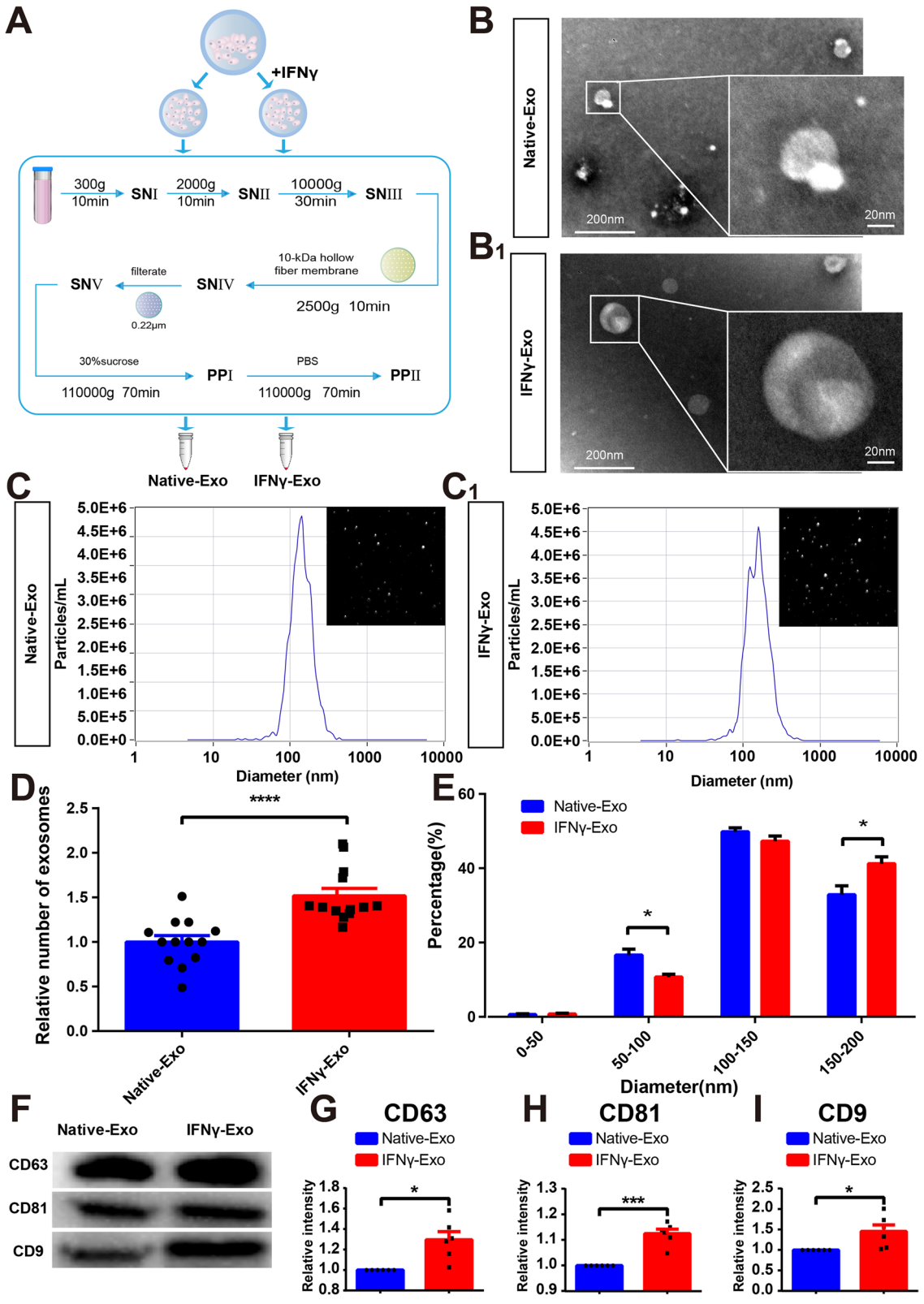

Fig. 1 (See legend on previous page.)

days postnatal (P21). Equal volumes of phosphate-buffered saline (PBS) were injected into the vitreous cavity of RCS rats as a control. Flash electroretinogram (FERG) analysis was performed at 2, 4, 6, and 8 weeks after injection according to previous research [21, 52]. The test flow chart is shown in Fig. 2A. After analyzing the retinal current response under 3.0 cd*s/m^2 light intensity, we found that the amplitudes of the a and b waves in the Native-Exo and IFNγ-Exo groups were significantly higher than those in the PBS group at 2 weeks after injection. The amplitude of the b-wave in the IFNγ-Exo group was significantly higher than that in the Native-Exo group, whereas there was no significant difference in the amplitude of the a-wave between these two groups (Fig. 2B–D). The amplitudes of the a and b waves in the Native-Exo and IFNγ-Exo groups at 4 and 6 weeks after surgery were significantly improved compared with those in the PBS group. Moreover, the amplitudes of a and b waves in the IFNγ-Exo group were significantly higher than those in the Native-Exo group at 4 and 6 weeks after surgery (Fig. 2E–J). Similar effects were observed in the amplitude of the b-wave at 8 weeks after IFNγ-Exo or Native-Exo injection, however, pairwise comparison of the amplitude of the a-wave between the three groups showed that only the amplitude of the IFNγ-Exo group was significantly higher than that of the PBS group (Fig. 2K–M). Collectively, these findings suggest that exosomes in the IFNγ-Exo and Native-Exo groups can restore retinal function, with the protective effect of exosomes found to be improved by IFNγ stimulation, lasting from 2 to 8 weeks after injection.

IFNγ-Exos protects photoreceptor survival in RCS rats

The difference in retinal function protection between IFNγ-Exo and Native-Exo groups was most significant 4 weeks after exosome injection. The exosomes were only a small amount distributed in the outer nucleus layer (ONL) at this time point (Fig. 3A). The thickness of the ONL in the IFNγ-Exo and Native-Exo groups (position 1, -1, 2) was thicker than that in the PBS group. In some positions (-3, -2, -1, and 1) of the retina, the thickness of the ONL in the IFNγ-Exo group was greater than that in the Native-Exo group (Fig. 3B). In addition, TUNEL staining showed that the apoptotic cells were mainly distributed in the ONL of RCS rats (Fig. 3C). Moreover, the number of TUNEL-positive cells in the ONL of the two exosome injection groups was significantly lower than that in the PBS group, which was more obvious in the IFNγ-Exo group (Fig. 3C, D). Rhodopsin is a cell marker of photoreceptors, and our experimentsshowed that its fluorescence intensity in the two exosome injection groups was higher than that of the PBS group, and the area of the IFNγ-Exo group was significantly higher than that of the Native-Exo group (Fig. 3E, F). These findings suggest that IFNγ treatment enhances the protective effect of MSC-derived exosomes on degenerative photoreceptors.

Expression profile of tRFs and tiRNAs in IFNγ-Exos

To explore the mechanism by which IFNγ-Exo is more effective in delaying RP development, the tRF and tiRNA levels in exosomes were analyzed using high-throughput sequencing technology.

The quality score plots display that the quality score of each sample is above 30, meeting the quality control of tRF and tiRNA sequencing (Figure S3A-F). The correlation coefficient shows that samples within the same group have high similarity, while samples among groups have notable variations (Figure S3G). Venn diagram presents that The number of detected tRFs and tiRNAs was 1069, and no tRFs and tiRNAs was identified in the database (Figure S3H). The significant differences in the expression of tRFs and tiRNAs in exosomes between the IFNγ-Exo and Native-Exo groups were shown by principal component analysis (Fig. 4A). There were 387 tRFs and tiRNAs present in both IFNγ-Exo and Native-Exo groups, while 217 and 27 tRFs and tiRNAs were unique to the IFNγ-Exo group and Native-Exo group, respectively (Fig. 4B). In addition, tRF-3a, tRF-3b, and tRF-2 were detected in the IFNγ-Exo exosomes instead of in the Native-Exo group (Fig. 4C). The stacking diagram shows that tRNAs can produce a type of tRF or tiRNA by splitting into fragments with the same sequence (Fig. 4D). The frequencies of subtype against the length of the tRFs

(See figure on next page.)

Fig. 2 IFNγ pretreated exosomes protect retinal function in RP rats. **A** Chart of exosome infusion and schematic of the time point of the retinal function test. **B** Representative waveforms of the FERG test 2 weeks after exosome infusion at 3.0 cd*s/m^2 light intensity. **C**, **D** Comparison of a and b wave amplitudes at 2 weeks after exosome infusion ($n > 10$). **E** Representative waveforms of the FERG test 4 weeks after exosome infusion at 3.0 cd*s/m^2 light intensity. **F**, **G** Comparison of a and b wave amplitudes at 4 weeks after exosome infusion ($n > 10$). **H** Representative waveforms of the FERG test 6 weeks after exosome infusion at 3.0 cd*s/m^2 light intensity. **I**, **J** Comparison of a and b wave amplitudes at 6 weeks after exosome infusion ($n > 10$). **K** Representative waveforms of the FERG test 8 weeks after exosome infusion at 3.0 cd*s/m^2 light intensity. **L**, **M** Comparison of a and b wave amplitudes at 8 weeks after exosome infusion ($n > 10$). Data represent the mean ± SEM. ns: No significant difference, $*P < 0.05$, $**P < 0.01$, $***P < 0.001$, $****P < 0.0001$

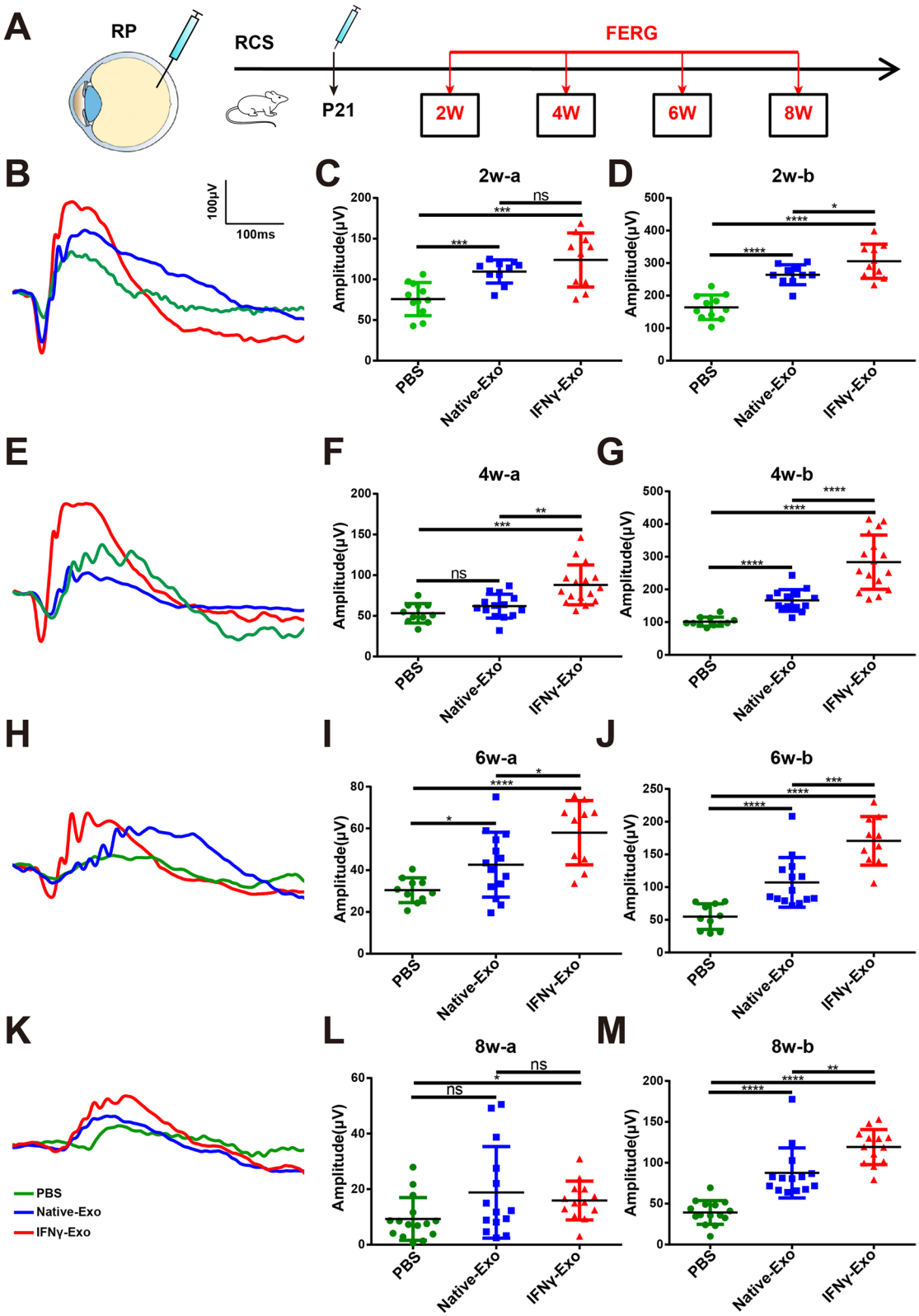

Fig. 2 (See legend on previous page.)

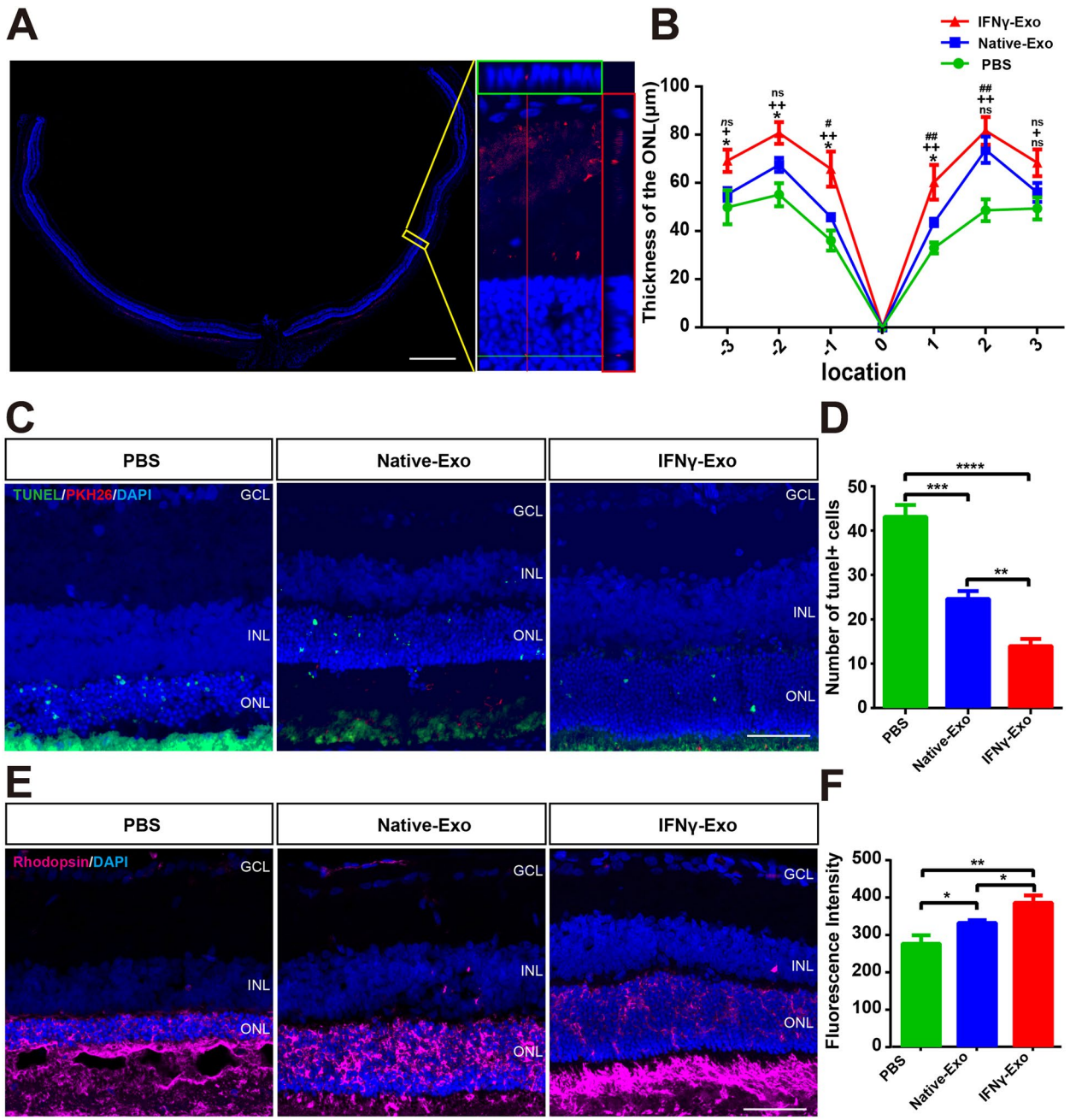

Fig. 3 IFNγ pretreated exosomes protect photoreceptors in RCS rats. **A** Whole retinal montage and partial enlargement of PKH26 stained exosomes in the retina at 4 weeks after injection. **B** Quantification of ONL thickness at different positions of the retina in differently treated groups of rats ($n=6$). **C** Immunofluorescence staining images of TUNEL staining (green), PKH26 (Red) and DAPI (blue) of the three retinal groups. **D** Comparison of the numbers of TUNEL-positive cells in one field of the retina in the two treatment groups ($n=5$). **E** Representative images of immunofluorescence for specific markers of photoreceptor cells (purple) and DAPI (blue) in the rat retina showing Rhodopsin expression in the three groups. **F** Quantitative analysis of the area of Rhodopsin expression in the three groups shown in (E) ($n=5$). Positions−1 and 1: Both sides of the optic disk, Positions−2 and 2: The middle of the optic disk and the ciliary margin, Positions−3 and 3: Marginal position of the retina. GCL: Retinal ganglion cell layer, INL: Inner nuclear layer, ONL: Outer nuclear layer. #: PBS vs. Native-Exo; +: PBS vs. IFNγ-Exo; *: Native-Exo vs. IFNγ-Exo. Data represent the mean ± SEM; ns: No significant difference, ∗$P<0.05$, ∗∗$P<0.01$, ##, $P<0.01$;++$P<0.01$, ∗∗∗$P<0.001$, ∗∗∗∗$P<0.0001$. Scale bars: whole retinal map, 500 μm; enlarged view, 50 μm; C, E 50 μm

and tiRNAs in the two groups (Fig. 4E). Figure S4A–F shows the relationship between the total reading and the length of the trim reading.

Differential expression of tRFs and tiRNAs in IFNγ-Exo

Under the truncation criteria of fold change ≥ 1.5 and $P < 0.05$, 224 differentially expressed tRFs/tiRNAs were observed in the IFNγ-Exo group compared with the Native-Exo group. Among them, 120 were upregulated and 104 were downregulated (Fig. 5A, S5). The unsupervised hierarchical clustering heatmap shows the significant difference of tRF and tiRNA expression profiles in the IFNγ-Exo and Native-Exo groups (Fig. 5B). After excluding the type of pre- and chrM-tRFs and tiRNAs, we predicted the target genes of the top 50 differentially expressed tRFs and tiRNAs. And 1830 target mRNAs for 28 DE tRFs/tiRNAs were identified using RNA Hybrid and miRanda algorithms. GO analysis showed that these target genes were mainly related to Wnt signaling and metabolism (Figure S6A). And KEGG pathway analysis confirmed that target genes mainly converged on inflammatory and immune-related pathways, including the Ras, mTOR, Chemokine, and Wnt signaling pathways (Figure S6B). This suggests that IFNγ treatment alters the tRF expression profile of MSC exosomes, which may disturb immune and inflammation-related pathways.

To further explore effective molecules of research significance (length > 16 nt), the following three, which were related to immune inflammation, were selected: Other-1_17-tRNA-Phe-GAA-1-M3, Other-6_23-tRNA-Lys-TTT-3, and TRF-57:75-GLN-CGG-2-m2. These three tRFs and tiRNAs were only expressed in the IFNγ-Exo group and not in the Native-Exo group (Fig. 5C). The criterion for target gene prediction was a structure score ≥ 140. The target genes were selected to construct the Other-1_17-tRNA-Phe-GAA-1-M3, Other-6_23-tRNA-Lys-TTT-3, and TRF-57:75-GLN-CGG-2-m2 networks. It showed that the target genes of the three tRFs and tiRNAs were also involved in inflammatory and immune-related pathways, such as EGFR tyrosine kinase inhibitor resistance, mTOR signaling pathway, and Wnt signaling pathway (Fig. 5D). Thus, IFNγ-Exo may achieve better protective effects on the retinal function and photoreceptors in the degenerative retina mainly through immune and inflammatory regulation.

IFNγ-Exos regulates the immune microenvironment in the retinas of RCS rats

Because microglia play an important role in the regulation of the immune microenvironment associated with retinal inflammation [53, 54], we observed that PKH26-labeled MSC-Exos colocalized with Iba1-labeled retinal microglia 4 weeks after injection (Fig. 6A). In both the IFNγ-Exo and Native-Exo groups, there was a notable reduction in the number of microglia labeled with Iba1 in the retinas of RCS rats compared to the PBS group. Moreover, the decline observed in the IFNγ-Exo group was more substantial in comparison to the decrease witnessed in the Native-Exo group (Fig. 6B, C). As previously reported [1], we used grid analysis to characterize the morphological differences in microglial cells (Fig. 6D). The results showed that the grid cross point of microglia in the IFNγ-Exo group was significantly higher than that in the Native-Exo group in both the full layer of the retina (Fig. 6E) and the outer retina (ONL and SSR) (Fig. 6F), whereas there was no significant difference in the inner retina (Fig. 6G).

We then analyzed the CD86 and Iba1 double-stained microglia in the retina and found that the number of CD86/Iba1 double-stained microglia was significantly decreased in both the IFNγ-Exo and Native-Exo groups, and that the number of CD86/Iba1 double-stained cells in the IFNγ-Exo group was less than that of the Native-Exo group (Fig. 7A, B). CD206 was selected as a signature protein to analyze microglia homeostasis, and immunostaining showed that the number of CD206-positive microglia was increased in the IFNγ-Exo group compared to that in the Native-Exo group (Fig. 7C, D). Furthermore,

(See figure on next page.)

Fig. 4 tRFandtiRNAprofiles of exosomes isolated from IFNγ-pretreated MSCs. **A** Primary component analysis. The three main factors that influenced the expression level of the sample are represented by the X, Y, and Z axes. Each colored point signifies a specific sample and its position reflects the primary characteristic of that sample. The spatial distance is indicative of the similarity in data size. **B** The number of commonly and specifically expressed tRFs and tiRNAs is represented in this Venn diagram. It illustrates the presence of tRFs and tiRNAs in both groups, as well as their specific expressions. **C**, **C_1** Distribution of tRF and tiRNA subtypes. The colors represent the tRF and tiRNA subtypes. The values in brackets represent the numbers of tRF and tiRNA subtypes. **D**, **D_1** The number of subtypes of tRFs and tiRNAs against tRNAs is decoders. The X-axis represents tRNAs is decoders, and the Y-axis shows the number of all subtypes of tRFs and tiRNAs against tRNAs is decoders. The color represents the subtypes of tRFs and tiRNAs. **E**, **E_1** The frequency of subtypes against the length of tRFs and tiRNAs is depicted in the graph. The X-axis represents the length of the tRFs and tiRNAs, while the Y-axis shows the frequency of the subtypes. The color in the graph represents the different subtypes of tRFs and tiRNAs

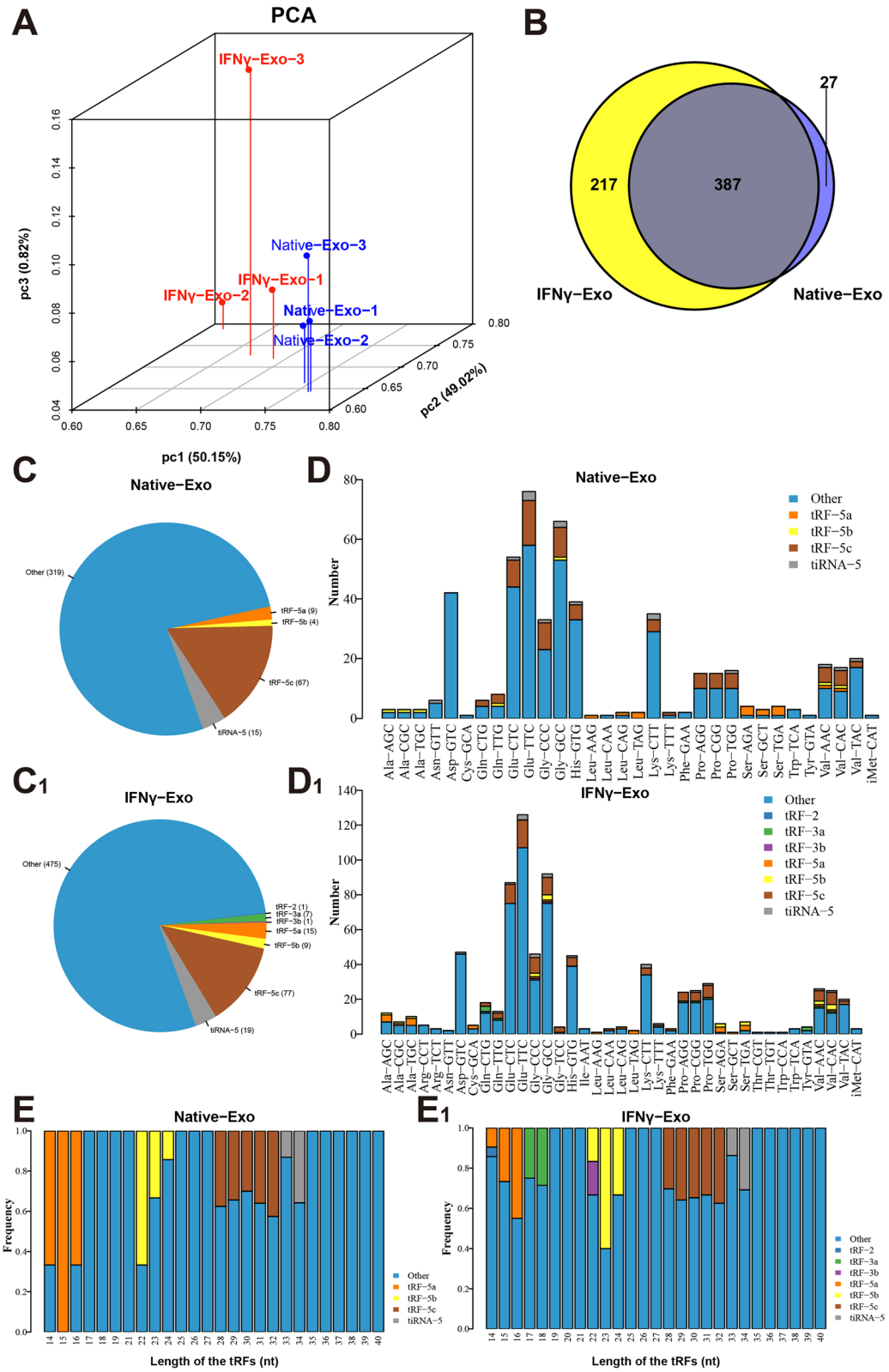

Fig. 4 (See legend on previous page.)

exosomes significantly inhibited the expression of the proinflammatory genes IL-1β, TNF-α, IL-6, iNOS, and the effect of the IFNγ-Exo group was better than the Native-Exo group (Fig. 7E–H). Other-1_17-tRNA-Phe-GAA-1-M3 exhibited the highest expression level and the greatest difference in expression of the above three important effective small RNA molecules. Src is an important target gene of Other-1_17-tRNA-Phe-GAA-1-M3. Interestingly, Src expression was not affected by Native-Exo, whereas it was significantly increased by IFNγ-Exo (Fig. 7I). These findings suggest that exosomes inhibit the overactivation of microglia in the degenerative retina and reduce retinal inflammation, and that IFNγ-Exo treatment is more effective than Native-Exo treatment.

IFNγ-Exos regulate the cellular immune response of BV2 cells

To further verify the effect of exosomes on microglia, BV2 cells were cultured with LPS and freshly extracted PKH26-labeled exosomes. The results showed that exosomes were engulfed by BV2 cells at 0.5 h, and almost all exosomes were engulfed by microglia at 4 h (Fig. 8A). BV2 cells were treated with 1 μg/mL LPS for 24 h, and then IFNγ-Exos and Native-Exos were added and maintained for 24 h. The three-dimensional reconstruction revealed that the exosomes were encased in the cytoskeleton (Fig. 8B). LPS treatment activated the BV2 cells, and the cytoskeleton became short and cluttered (Fig. 8C). CCK-8 analysis showed no significant differences in cell activity among all groups (Fig. 8D). IFNγ-Exo treatment significantly upregulated the LPS-induced decline in Src expression, while there was no significant difference in Src expression between the Native-Exo + LPS and LPS-treated groups (Fig. 8E). LPS stimulation also significantly increased the expression of IL-1β, TNF-α, IL-6, and iNOS in BV2 cells, whereas exosome treatment significantly downregulated the expression of these proinflammatory genes in both groups, with IFNγ-Exo treatment showing the greatest effect (Fig. 8F–I). Therefore, these results suggest that IFNγ-Exos produces a better anti-inflammatory effect on LPS-activated microglia cells than Native-Exo in vitro.

Other-1_17-tRNA-Phe-GAA-1-M3/Src plays a key role in the enhanced anti-inflammatory effect of IFNγ-Exos

Among the three tRNAs discussed above, both the expression level and the difference in the expression of Other-1_17-tRNA-Phe-GAA-1-M3 were higher than those of Other-6_23-tRNA-Lys-TTT-3 and TRF-57:75-GLN-CGG-2-M2. Mimics were synthesized based on the sequences of Other-1_17-tRNA-Phe-GAA-1-M3. BV2 cells were activated through 24-hour LPS treatment. Src was then knocked down in some of the BV2 cells with lentivirus, after which the mimics were added to the two types of BV2 cells. The results showed that LPS activation caused cytoskeleton disorder in BV2 cells, which was significantly improved after the addition of the mimics. However, this effect was blocked by Src knockdown (Fig. 9A, B). Moreover, the mimics significantly inhibited the levels of the inflammatory factors IL-1β, TNF-α, IL-6, and iNOS, and the anti-inflammatory effect was blocked after Src knockdown (Fig. 9C–F). This suggests that Other-1_17-tRNA-Phe-GAA-1-M3 mimics improve LPS-evoked microglia activation through the upregulation of Src expression.

Discussion

RP is a group of hereditary disorders affecting the retina, and microglia activation has been observed in both experimental and clinical instances of RP [55, 56]. In the current study, we found that BMSC-Exos significantly improved the activation status of microglia. Importantly, after treatment with IFN-γ, this effect became stronger and was also more effective in protecting the degenerative retina of RP rats. Our results showed that IFNγ pretreatment increased the expression of CD81 and CD9 and the particle size and quantity of exosomes. In-depth analysis showed that the high expression of the tsRNA

(See figure on next page.)

Fig. 5 Differential expression (DE) analysis of tRF and tiRNA expression profiles in exosomes derived from IFNγ-treated MSCs. **A** Volcano plot of tRFs and tiRNAs. The values of the X and Y axes in the volcano plot are $\log_2$ transformed fold change and $\log_{10}$ transformed p-values between the two groups, respectively. Circles colored in red or blue signify statistically significant differentially expressed tRFs and tiRNAs, displaying a fold change of 1.5 and a *p*-value of ≤ 0.05 (red indicates up-regulation, while blue indicates down-regulation). On the other hand, circles colored in gray denote non-differentially expressed tRFs and tiRNAs, implying that their fold change and/or q-value fail to meet the determined cutoff thresholds. **B** Unsupervised hierarchical clustering heatmap for tRFs and tiRNAs. The color in the panel represents the relative expression level ($\log_2$-transformed): blue represents an expression level less than the mean, and red represents an expression level greater than the mean. The colored bar on the right side of the panel indicates the divisions that were performed using K-means. **C** Comparison of CPM values of three tRFs. **D** The network of the tRF-mRNA pathway, including Other-1_17-tRNA-Phe-GAA-1-M3, Other-6_23-tRNA-Lys-TTT-3, and TRF-57:75-Gln-CTG-2-m2, 77 mRNAs, and 10 pathways. Orange represents tRFs, cyan represents mRNA, and blue represents the pathway

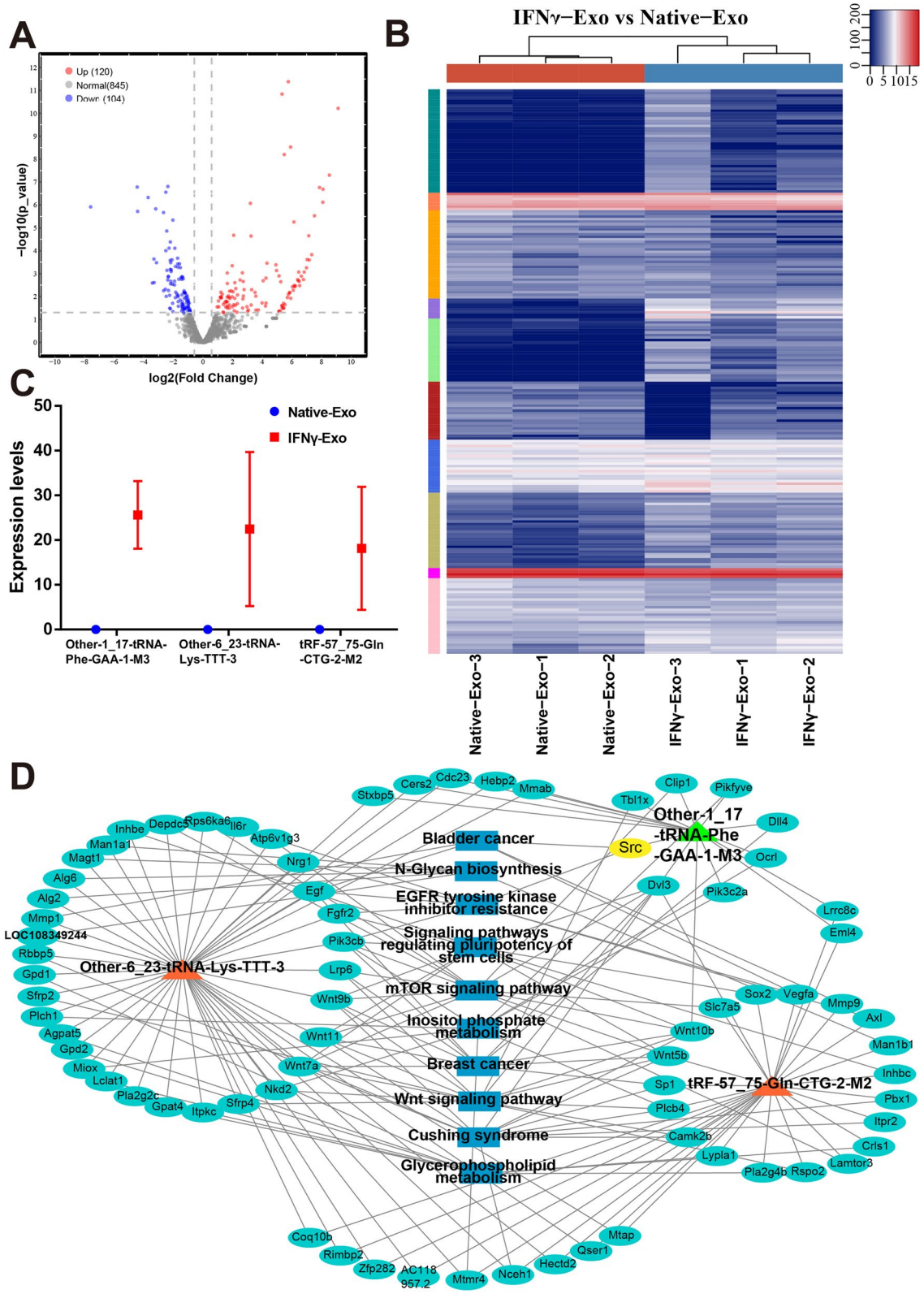

Fig. 5 (See legend on previous page.)

Other-1_17-tRNA-Phe-GAA-1-M3 in the exosomes of the IFNγ-treated group was regarded as targeted to regulate the expression of Src, which may serve to modulate the immune status of microglia. By adding Other-1_17-tRNA-Phe-GAA-1-M3 mimics to the microglia culture system and targeting Src expression, we further demonstrated that the regulation of Src by Other-1_17-tRNA-Phe-GAA-1-M3 improved microglial activation.

MSCs have promising efficacy for treating retinal degeneration, partially through the regulation of microglia or macrophages [57, 58]. IFNγ, a cytokine secreted by activated natural killer (NK) cells and T cells, serves as a pivotal player in adaptive immune responses [59]. MSCs that have been stimulated with IFN-γ demonstrate potent immunomodulatory effects by inducing the elevation of immune-activating molecules [27]. Nevertheless, there remains a significant knowledge gap regarding alterations in microglial subtypes after treatment with exosomes derived from IFNγ-pretreated MSCs and the functional improvement in RCS rats. Our findings indicated that IFNγ induces MSCs to produce more exosomes with larger diameters, and the expression of the exosomal signature protein CD9 was significantly upregulated, which was consistent with the report of Zhang's group [60]. Our results demonstrated that injection of IFNγ-Exos into the vitreous body of RCS rats produced better protection of photoreceptors and retinal functions than the native MSC-derived exosomes. This is consistent with the findings of a previous report, in which exosomes derived from human MSCs stimulated by IFNγ produced better therapeutic effects on EAE mice [18]. These findings suggest that IFNγ preconditioning may represent a strategy to optimize the exosomes of MSCs, providing new insight into improving exosome performance for treating related diseases.

To explore the mechanisms underlying the neuroprotective effect of IFNγ-Exos on RCS rats, we compared the proteomic cargo between IFNγ-Exos and Native-Exos. As functional small non-coding RNAs, tRFs and tiRNAs are abundantly distributed in exosomes and maintain a stable structure and highly conserved characteristics [39, 61]. In this study, we demonstrated that three tRFs and tiRNAs were highly expressed in IFNγ-Exos; it was related to neuroinflammation. Among them, the expression level of Other-1_17-tRNA-Phe-GAA-1-M3 was the highest. Given the large number of tRFs that were significantly different between IFNγ-Exos and Native-Exos, we performed target enrichment analysis to investigate the targets of the complete EV tRF cargo. The top targets of the IFNγ-Exo-tRF cargo included Src and several genes involved in cell proliferation, migration, and development, such as the adaptor protein transducing beta-like 1 (TBL1X), the Clip1, and the ligand Delta-like 4 (Dll4).

Src is an important target gene of Other-1_17-tRNA-Phe-GAA-1-M3, which modulates the MAPK pathway, and MAPK regulates macrophage activation, cytokine production, and chemotaxis [62]. Notably, Src-related signaling participates in the factor-regulated interaction between inflammatory cells. Src is sufficient for developing microgliosis [63]. tRFs and tiRNAs exhibit various biological functions through multiple mechanisms, including interactions with proteins or mRNA, gene expression regulation, cell cycle modulation, intercellular communication, and involvement in chromatin and epigenetic modifications [48, 61, 64–67]. In the present study, Other-1_17-tRNA-Phe-GAA-1-M3 was observed to upregulate Src expression. It has been suggested that tsRNAs may enhance gene expression by attenuating gene silencing, as they compete with miRNAs/mRNA for incorporation into RNA-binding proteins (RBPs) (e.g. YABX1), thereby forming essential components in RNA-induced silencing complexes (RISC) [68, 69]. Moreover, recent research indicates that tRFs, which exhibit miRNA-like functions, can induce mRNA conformational changes, which in turn promote tsRNA to bind to partially complementary sequences within target genes, thus enhancing mRNA stability and translation [70, 71]. Nevertheless, the precise mechanism by which Other-1_17-tRNA-Phe-GAA-1-M3 regulates Src mRNA remains unclear; thus, further investigations are needed to elucidate the regulatory network involving tRFs. An in-depth study of the function and regulatory mechanism of tsRNAs will help reveal its role in biology and medicine, as well as its role in disease diagnosis and treatment, which will be our major research direction in the future.

(See figure on next page.)

Fig. 6 IFNγ-pretreated exosomes inhibit microglia activation in the retina of RCS rats. **A** Whole retinal montage and partial enlargement of the colocalization of Iba1-labeled microglia and PKH26-labeled exosomes. **B** Representative images of immunofluorescence for specific markers of microglia (green) and DAPI (blue) in the rat retina showing Iba1 expression in the three groups. **C** Quantitative analysis of the number of Iba1-positive cells expressed in the three groups shown in (B) ($n=5$). **D** Three groups of representative grid cross images of Iba1-labeled microglial immunofluorescence morphogram. **E–G** Comparison of the number of microglial cell grid intersections at different locations in the three retina groups: E. Grid cross point in the whole retina, F. Grid cross point in the ONL and SSR, and G. Grid cross point in the inner retina ($n=5$). SSR: Subretinal cavity, GCL: Retinal ganglion cell layer, INL: Inner nuclear layer, ONL: Outer nuclear layer. Data represent the mean ± SEM. ns: No significant difference, ∗$P<0.05$, ∗∗$P<0.01$, ∗∗∗∗$P<0.0001$. Scale bars: whole retinal map, 500 μm; enlarged view, 50 μm; B 50 μm; Grid diagram, 10 μm

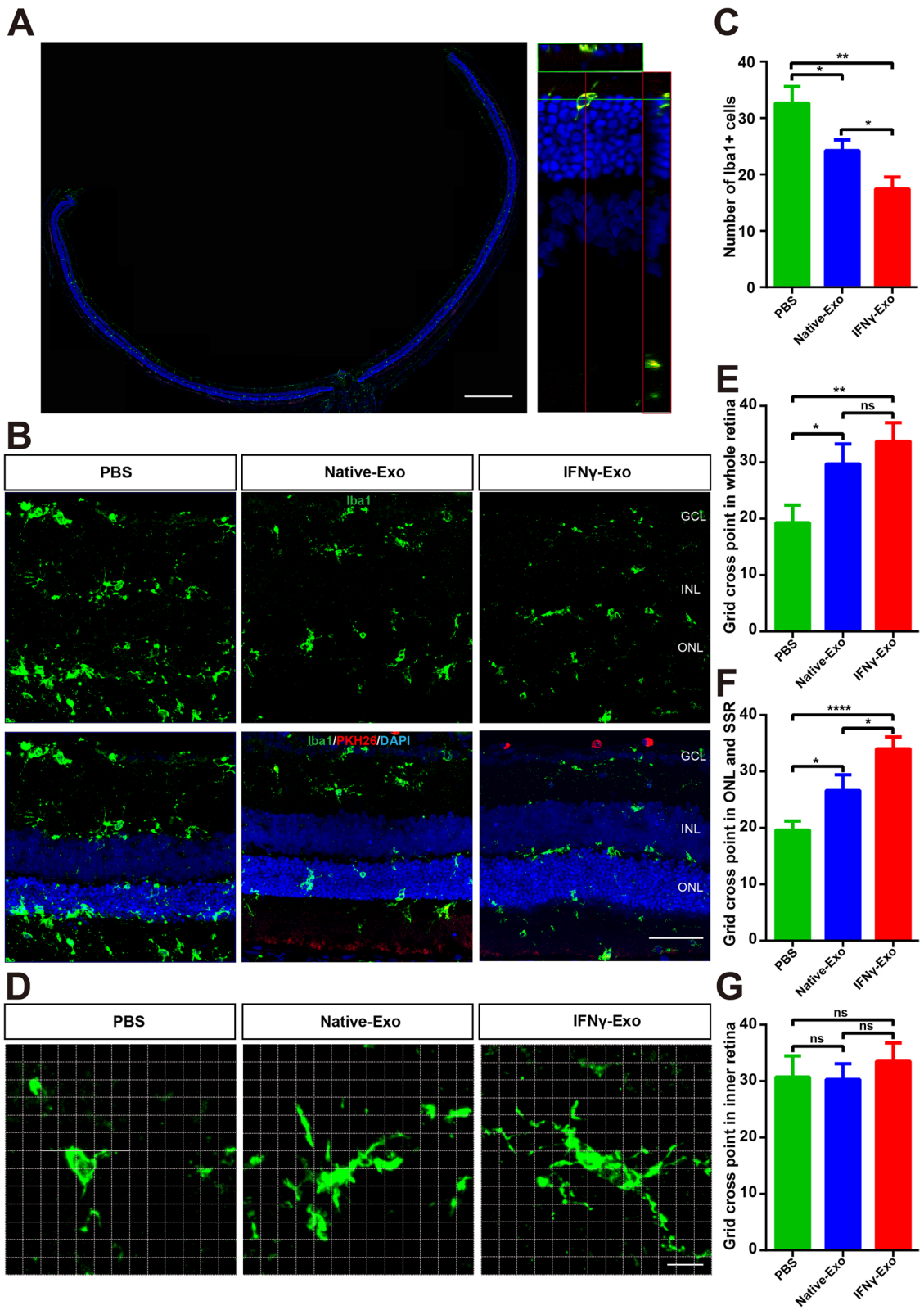

Fig. 6 (See legend on previous page.)

Microglia, which are immune cells situated in the retina, play a crucial role in RP development. New investigations have uncovered the potential of varied phenotypic expressions in microglia, rendering them highly diverse and adaptable. The manifestation of these phenotypes is contingent upon the disease's severity and stage, as well as the distinct inflammatory environment [72]. Our previous research demonstrated that resident microglia in the OPL effectively inhibit ectopic neurogenesis and delay vision deterioration by engulfing synapses in the early stages of RP [73]. Furthermore, the activation of disease-associated microglia (DAM) in the outer retina of RCS rats reduces secondary photoreceptor degeneration caused by the accumulation of dead cells and infiltrated neutrophils [74]. These findings suggest that microglia can respond to various photoreceptor insults and transform into different phenotypes, both pro- and anti-inflammatory, each exerting distinct functions [74]. Therefore, redirecting microglial activation toward beneficial and neuroprotective phenotypes has the potential to halt the progression of RP.

To verify the regulatory effect of IFNγ-Exos on microglia, we injected them into the vitreous body of RCS rats and co-cultured them with LPS-induced BV2 microglia in vitro. The results demonstrated that IFNγ-Exos promoted activated microglia polarization to homeostasis and inhibited the expression of proinflammatory genes in vivo. Importantly, treatment with IFNγ-Exos significantly upregulated LPS-induced Src expression. We also used lentivirus and mimics to knock down Src expression and found that the anti-inflammatory effect of IFNγ-Exos was blocked. Hence, our results suggest that Other-1_17-tRNA-Phe-GAA-1-M3/Src may represent a novel target in the investigation of IFNγ-Exo treatment, implying a potential molecular mechanism by which IFNγ-Exos polarizes microglia homeostasis in RP.

Next, to establish whether IFNγ-Exos have immune-regulatory functions, we injected them into the vitreous body of RCS rats. For the in vitro experiments, we chose BV2 microglia and used LPS to induce microglial neuroinflammation in vitro. Microglia can exert double-edged effects depending on their intrinsic subtypes, including disease-associated and homeostasis phenotypes. A previous study demonstrated that miR-124 could reduce inflammation by modulating microglial polarization in intracerebral hemorrhage [75]. Dou et al. proved that MSC-Exos inhibited the M1-type polarization of macrophages, possibly by transferring tsRNA-21,109, in systemic lupus erythematosus [50]. In this study, the IFNγ-Exo group was shown to promote microglia to restore homeostasis and reduce pro-inflammatory cytokines both in vivo and in vitro. Based on these results, we conclude that IFNγ-Exos represents a promising bioagent to improve functional behavioral recovery by promoting the microglia to restore homeostasis in RCS rats.

To better understand the phenomenon underlying the ability of IFNγ-Exos to promote microglia to restore homeostasis in vivo and in vitro, we chose the target tsRNA Other-1_17-tRNA-Phe-GAA-1-M3 and its target gene Src for further study. Src kinases are present in glial cells and are upregulated following neurological insults in both human and animal models. BV2 were activated and showed increased TNF-a levels, which were attenuated by a Src kinase inhibitor, suggesting that Src plays a role in neuroinflammation and microglia polarization [63]. A previous study on the retina showed that Src inhibition in an ischemia-reperfusion injury model significantly reduced microglial activation, changed the morphology of microglia to a resting phenotype, and prevented neuronal apoptosis [76]. We also performed loss-of-function experiments to further confirm Src as the target gene of the identified tsRNA. The results demonstrated that the knockdown of Src in BV2 cells could abolish the beneficial effects observed from the anti-inflammatory effect in IFNγ-Exos. Taken together, we conclude that exosomal Other-1_17-tRNA-Phe-GAA-1-M3 derived from IFNγ-pretreated MSCs can suppress microglial-induced neuroinflammation by promoting microglia from DAM to homeostasis and inhibiting Src expression in RCS rats.

Despite the significant potential of exosomes derived from MSCs for the treatment of neurodegenerative diseases, their clinical application is limited by several factors, including shorter effectiveness period than the MSCs, limited targeting capabilities, rapid clearance following administration, and inadequate payload [77]. The varying physiological states of MSCs can influence the therapeutic efficacy of the exosomes derived from them.

(See figure on next page.)

Fig. 7 IFNγ-pretreated exosomes inhibit the homeostasis of microglia subtypes in the retinas of RCS rats. **A**, **C** Representative immunofluorescence images for specific markers of microglia (green), Iba1(red), and DAPI (blue) in the rat retina showing that the retinas express CD86 (A in green) and CD206 (C in green) in the three groups. **B**, **D** Quantitative analysis of the numbers of CD86 (A), CD206 (C), and Iba1 co-target microglial expression in the three groups shown in (A, C) ($n = 5$). Data represent the mean ± SEM. $*P < 0.05$, $***P < 0.001$. **E–I** Real-time PCR analysis of the expression of IL-1β, TNF-α, IL-6, iNOS, and the important target gene Src ($n = 3$). GCL: Retinal ganglion cell layer, INL: Inner nuclear layer, ONL: Outer nuclear layer. Data represent the mean ± SEM. ns: No significant difference, $*P < 0.05$, $**P < 0.01$, $***P < 0.001$. Scale bars: 50 μm

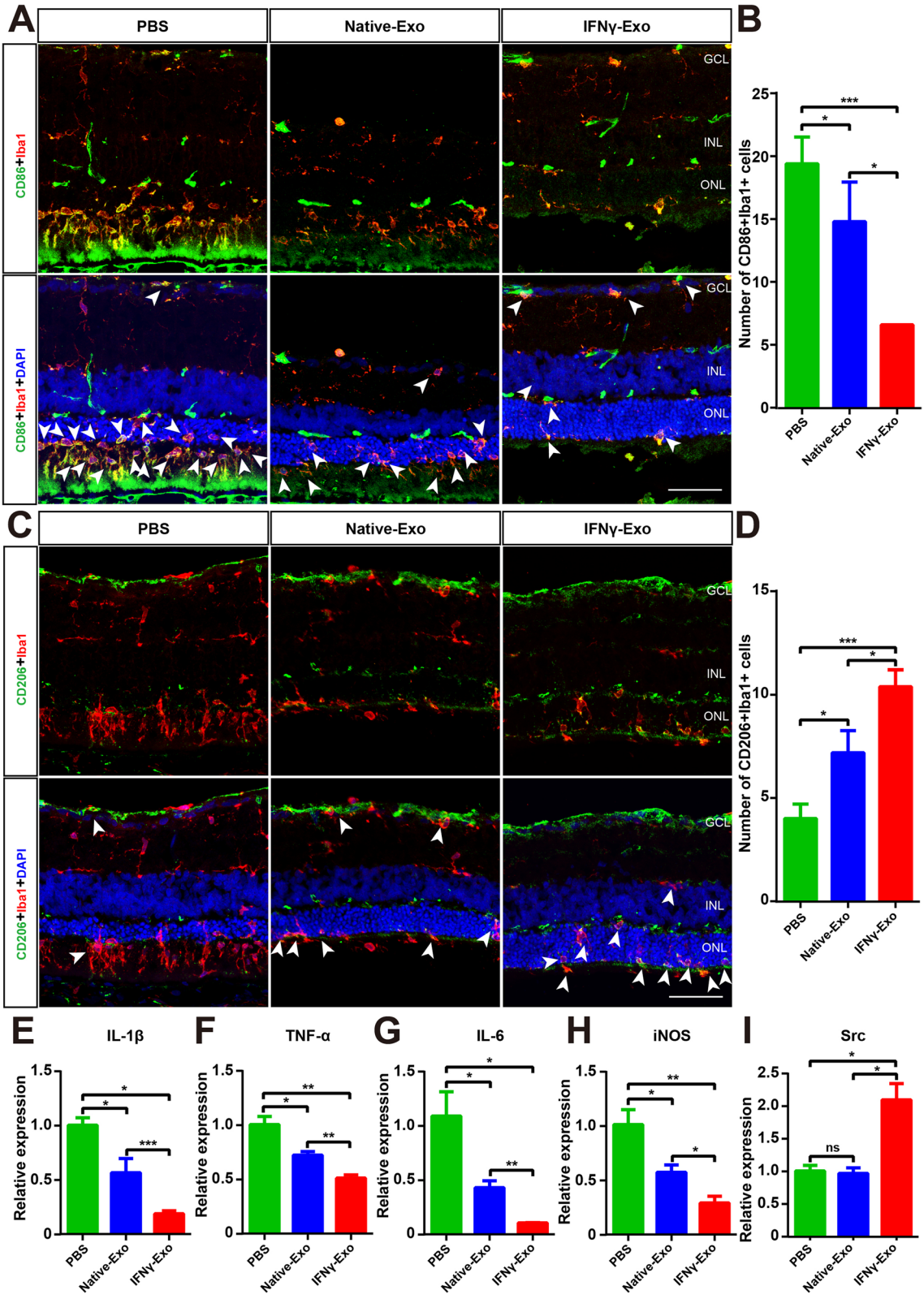

Fig. 7 (See legend on previous page.)

This issue may be partially addressed by using pre-conditioning techniques or by utilizing MSCs derived from induced pluripotent stem cells or embryonic stem cells, as these approaches may reduce the lot-to-lot variability commonly observed with primary naive MSCs [78]. Furthermore, it is essential to establish standards for the purity and quality control of isolated MSC-derived exosomes. It has demonstrated that different concentrations and durations of interferon- IFN-γ priming significantly impact the therapeutic effects of MSC-derived exosomes. It appears that limited enhancement in therapeutic effects was observed when utilizing low doses of IFN-γ for pre-conditioning [79]. In conclusion, the exploration of IFN-γ for the priming of MSCs remains an active area of investigation, with notable variability in methodologies employed across various studies. Despite this variability, there is a general consensus that priming MSCs with IFN-γ concentrations ranging from 10 ng/mL to 100 ng/mL for a duration of 24 to 48 h can augment the therapeutic potential of these cells [80]. Further validation is required to establish a standardized IFN-γ priming protocol that can be consistently applied across diverse studies and clinical applications.

Conclusion

In conclusion, our results suggest that MSC-Exo protects retinal photoreceptors and alleviates RP symptoms. Importantly, exosomes secreted by cells pretreated with IFN-γ produce better effects, which may be achieved by upregulating the expression of Other-52:71-tRNA-Ala-AGC-2 and TRF-57:75-GLn-Cgg-2-m2 in exosomes. tRFs and tiRNAs modulate inflammatory and immune-related pathways to inhibit microglial overactivation and retinal inflammatory responses. However, these conclusions need to be confirmed in the future by conducting simulation studies. Our findings not only provide new evidence for enhanced production and immune performance of MSC-derived exosomes but also provide a promising means to optimize the treatment of immune disorders and neurodegenerative diseases.

Materials and methods

Animals

Specific pathogen-free (SPF) grade RCS rats and their homologous normal rats (RCS-rdy$^+$) were provided (21 days after birth) and raised by the Experimental Animal Center of the Army Military Medical University. The environment was maintained in a 12-h light/dark cycle. All animal trials were approved by the Army Medical University Institutional Review Board, and all trials met guidelines. The production certificate number for our laboratory animal is SCXK-PLA-20,120,011, and the occupancy permit number is SYXK-PLA-20,120,031. All procedures in this study were approved.

Cell culture

As previously reported [81], bone marrow-derived MSCs were isolated and extracted from the femurs and tibias of RCS-rdy$^+$ rats 21 days after birth. Briefly, the bone marrow was flushed with pre-cooled phosphate-buffered saline (PBS), and all cells were collected by centrifugation and incubated in bone marrow mesenchymal cell complete culture medium (RAXMX-90011, Orilcell) in a 37 °C incubator filled with 5% CO_2. Two days later, the floating cells were washed with PBS and cultured. The cells were cultured to approximately 80–90% fusion and passed to the next generation. BV2 microglia cells were donated by Dr. Guo from the Department of Neurosurgery, Southwest Hospital [1] and cultured in Dulbecco's Modified Eagle Medium (SH30023.01B, Hyclone) containing 10% fetal bovine serum (FBS) (SH30406.05, Hyclone) in a 37 °C incubator containing 5% CO_2.

Purity and characterization of BMSCs

MSCs were identified according to current standards [82–84]. The cell morphology was observed under a light microscope and photographed. The surface markers of MSCs were analyzed by flow cytometry. Antibodies, such as CD11b, CD34, CD45, CD29, CD90, CD105, and CD44, were added to suspensions of 1×10^6 MSCs per tube, with allogenic nonimmune immunoglobulins used as controls, and incubated at 4 °C in the dark for 30 min. Following incubation, the cells were washed, resuspended, collected, and subjected to flow cytometry, before analyzing using FlowJo software (FlowJo 10.2). OriCell® Rat Bone Marrow Mesenchymal Stem Cell Osteogenic Differentiation Kit (RAXMX-90021, Orilcell) was used to detect the osteogenic differentiation ability of MSCs. After 14 days of culture according to the manufacturer's instructions, mineralization was measured with Alizarin

(See figure on next page.)

Fig. 8 IFNγ-pretreated exosomes inhibited activation of BV2 more efficiently. **A** Representative images of exosome phagocytosis by microglia at different times: (A) 0.5 h; A_1 1 h; A_2 4 h; A_3 24 h. **B** Three-dimensional reconstructions showing that exosomes are engulfed by microglia 24 h after addition. **C** Morphological images of phalloidin (purple), PKH26 (green), and DAPI (blue) in the four groups of BV2 cells 24 h after the addition of exosomes. **D** Comparison of cell viability in different groups by CCK-8 assay ($n = 5$). **E–I** Real-time PCR analysis of the expression of *Src*, *IL-1β*, *TNF-α*, *IL-6* and *iNOS* ($n = 3$). Data represent the mean ± SEM. ns: No significant difference, $*P < 0.05$, $**P < 0.01$. Scale bars: 10 μm

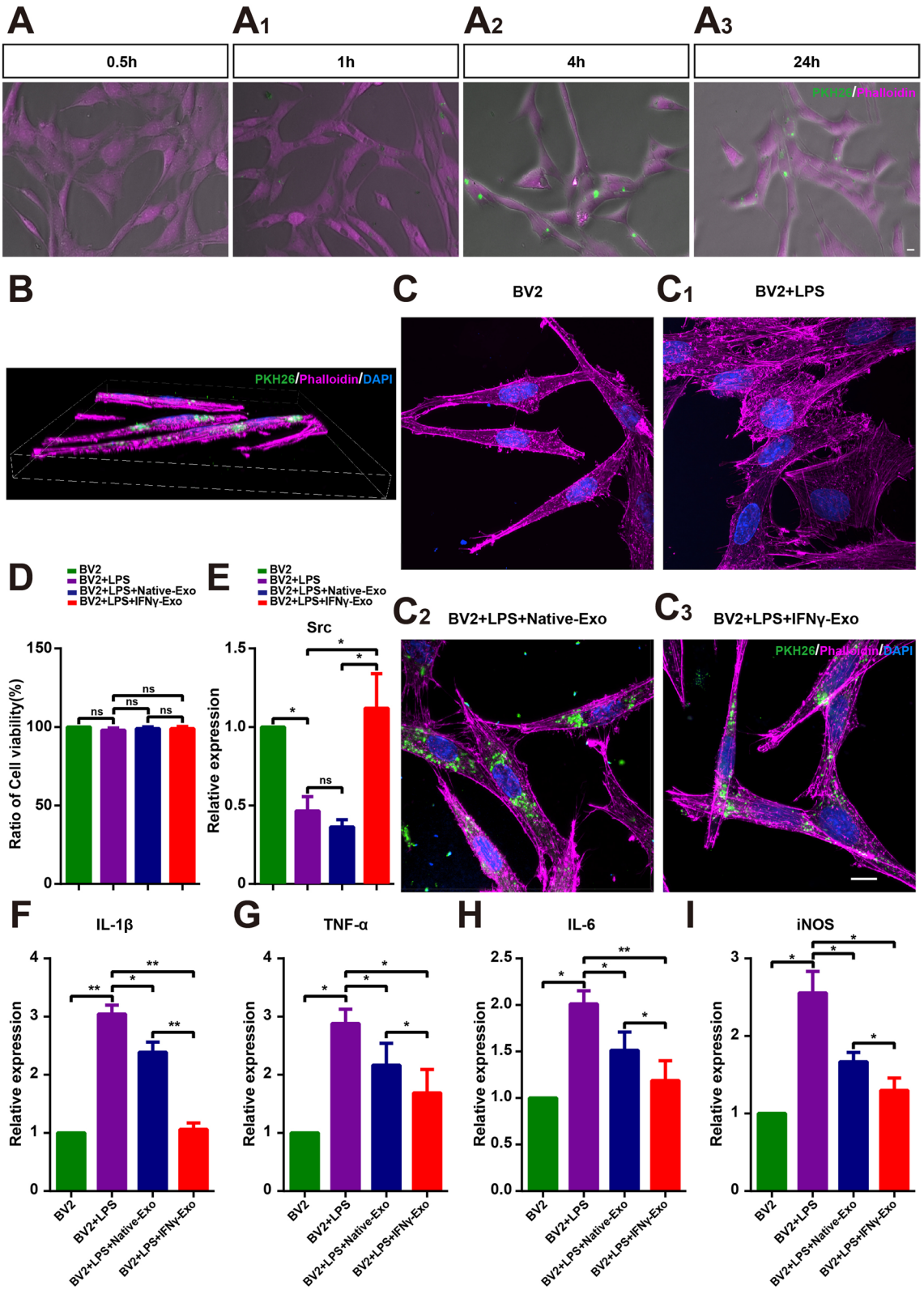

Fig. 8 (See legend on previous page.)

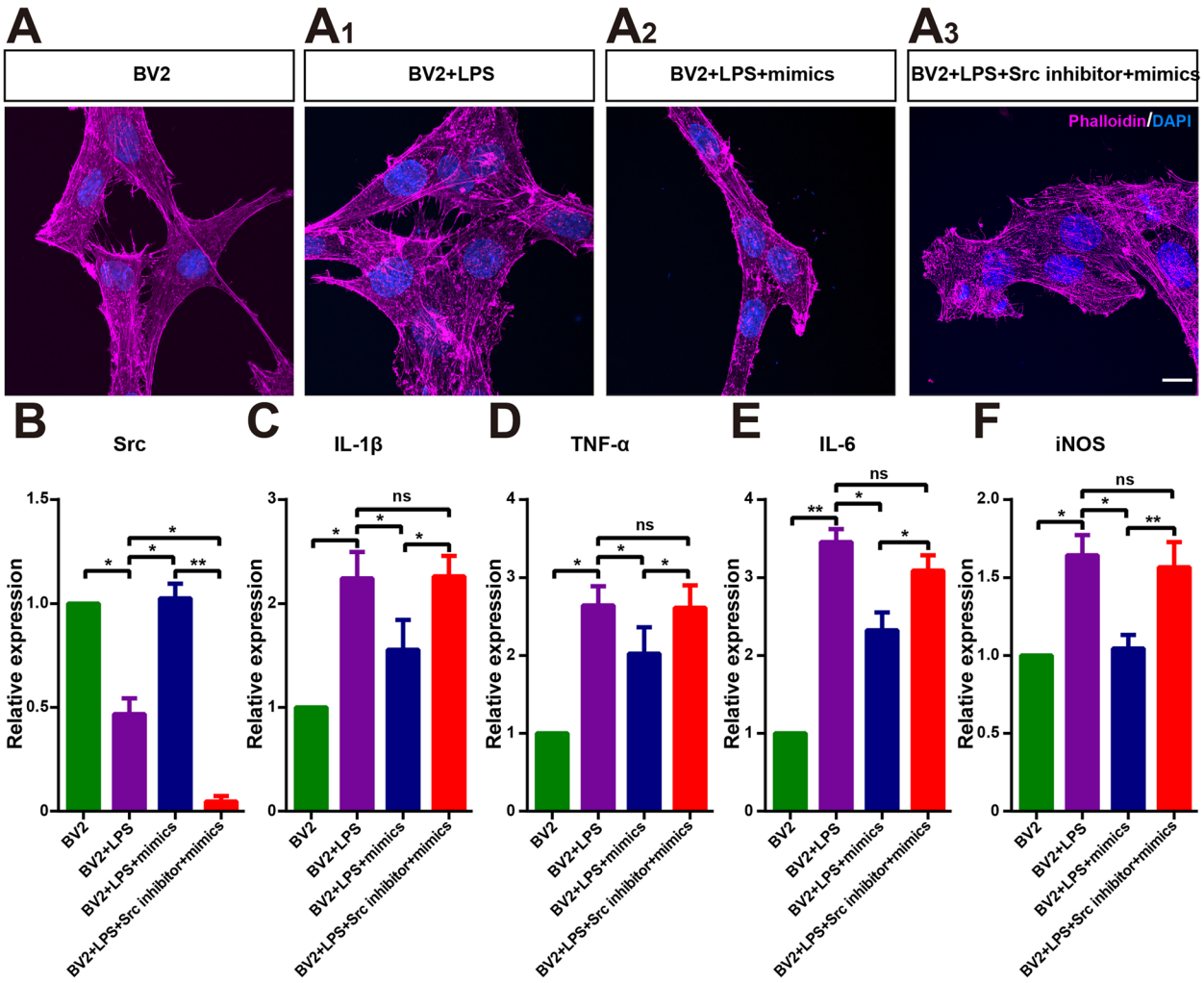

Fig. 9 Other-1_17-Trna-Phe-GAA-1-M3 mimics promote inhibition of BV2 activation by upregulating Src expression. **A-A$_3$** Morphological images of phalloidin (purple), PKH26 (green), and DAPI (blue) in the four groups of BV2 cells 24 h after the addition of mimics and Src inhibitors. **B–F** Real-time PCR analysis of *IL-1β*, *TNF-α*, *IL-6*, *iNOS* and src ($n = 3$). Data represent the mean ± SEM. ns: No significant difference, $*P < 0.05$, $**P < 0.01$. Scale bars: 10 μm

Red S contained in the kit. The OriCell® Rat Bone Marrow Mesenchymal Stem Cells Adipogenic Differentiation Kit (RAXMX-90031, Orilcell) was used to detect the adipogenic differentiation ability of MSCs. After 14 days of culture according to the instructions, mineralization was measured with the Oil Red O Solution contained in the kit. The chondrogenic differentiation ability of MSCs was determined using the OriCell® Rat Bone Marrow Mesenchymal Stem Cell Chondrogenic Differentiation Induction kit (RAXMX-90041, Orilcell). After 14 days of culture according to the manufacturer's instructions, the chondrocytes were made into frozen sections and stained with Alcian Blue 8GX Solution contained in the kit to detect chondrogenic differentiation. The differentiation of MSCs was observed using an optical microscope and photographed.

Exosome isolation

To stimulate MSCs, 50ng/mL recombinant rat IFNγ (598806, Biolegend) was added to the medium and incubated for 48 h. To isolate exosomes, the serum in the medium was replaced with exosome-depleted FBS (C38010050, VivaCell). MSCs were cultured in the exosome-free medium for 48 h, and the culture supernatants of stimulated and unstimulated cells were collected. As previously reported for exosome extraction [85], we first centrifuged the supernatant at 300 g for 10 min to remove the cells. The supernatant was further centrifuged at 2000 g for 10 min and 10,000 g for 30 min to

remove cell debris. Then, a hollow fiber membrane with 10-kDa interception molecular weight (Millipore) was used to concentrate the supernatant at 2,500 g for 10 min. The supernatant was then filtered through a 0.22-μm filter (Millipore) and centrifuged in a 30% sucrose cushion at 110,000 g for 70 min (SW 28Ti Swinging-Bucket Rotor, Beckman OPTIMA XPN-100). After carefully discarding the supernatant, PBS was added to wash the precipitate, before centrifuging again at 110,000 g for 70 min to collect the precipitate. Finally, the collected exosomes were precipitated with PBS. We used the ExoQuick-TC™ Exosome Precipitation Solution (EXOTC10A-1, System Biosciences) to separate exosomes according to the kit instructions.

Transmission electron microscopy (TEM)

The exosomes extracted from the rat BMSC culture supernatant were diluted with PBS, dropped on formvar-coated copper grids, and allowed to sit for 20 min at room temperature. The sample was then immersed in 2% polyformaldehyde, 2% glutaraldehyde, and 0.05 M phosphate solution and fixed for 2 min. Subsequently, the samples were washed with distilled water three times, before placing the copper mesh in 1% phosphotungstic acid redyeing for 1 min. After drying the copper mesh, TEM (JEM-1400PLUS, Japan) was used to observe and photograph the samples [52].

Nanoparticle tracking analysis (NTA)

Exosomes were extracted from two groups of cell culture supernatants of equal volume and simultaneous culture, and fresh exosomes were diluted with PBS buffer. The diluent was drawn with a 1-mL syringe and pushed into the detection chamber according to the ZetaView instrument (Particle Metrix, Germany) operating instructions, before recording and analyzing the dynamic image.

Western blotting (WB)

We performed WB analysis according to the method described previously [52, 86]. The extracted exosomes were cleaved in ice-cold tissue lysis buffer (1% PSMF + 99% RIPA). Protein was collected by centrifugation at 4 °C at 2000 g for 30 min. The bicinchoninic acid assay (BCA) (Beyotime, China) was used to determine the protein concentration according to the operating instructions. Equal numbers of exosomes from the two groups were loaded and separated on 12% SDS-PAGE gel. The electrophoretic conditions were as follows: 80 V accumulation and 100 V separation. The samples were then transferred to PVDF membranes and blocked in TBST buffer with 5% skim milk for 30 min. The membrane was then incubated with the primary antibody at 4 °C overnight, followed by incubation with the enzyme-labeled secondary antibody at room temperature for 1 h. Finally, according to the operating instructions, the protein bands were imitated by enhanced chemiluminescence (Amersham, Piscataway, NJ, USA), scanned by an Odyssey infrared imager system, and the protein staining was quantitatively analyzed by ImageJ software.

Cell viability assay

We performed a cell viability assay as described previously [86]. According to the Cell Counting Kit-8 (CCK-8; Dojindo Laboratory, Japan) instructions, we added 1×10^4 cells into one hole of the 96-well plate. The supernatant was removed and replaced with a 10:1 mixture of fresh serum-free medium and the CCK-8 kit. Incubation was performed at 37 °C for 1 h in the dark. Absorbance was measured at 450nm using a microplate reader (Varioskan Flash, Thermo Fisher).

Intravitreal injection

Intravitreal injection was performed as described previously [86, 87]. The concentrations of freshly extracted exosomes were measured by NTA assay, and the two groups were diluted to an equal concentration with PBS. The day that the rats were born was recorded as P0, and so on. At P21, the rats were anesthetized by intraperitoneal injection of 1% sodium solution of pelltobarbitalum natricum (Thermo Fisher, Waltham, MA, USA) (2.5mL/kg), and oxybuprocaine hydrochloride was added to perform ocular surface anesthesia. A total of 1×10^{11} exosomes were injected into the vitreous cavity with a microsyringe (33G; Hamilton, Bonaduz, Switzerland), and the same volume of PBS was injected into another eye as a control. After surgery, the eye surface was coated with tobramycin dexamethasone eye ointment (Dian Bishu), and the rats were placed back into the cage after recovery.

Electroretinogram (ERG)

Electroretinogram tests were performed as described above [88]. The rats were placed in a dark environment for at least 12 h before the experiment began. The rats were anesthetized by intraperitoneal injection of 1% sodium solution of pelltobarbitalum natricum (Thermo Fisher, Waltham, MA, USA) (2.5mL/kg) and placed on a 37 °C heating blanket to maintain body temperature. After applying tropicamide eye drops (Santen Pharmaceutical, Osaka, Japan) to the surface of the eye to dilate the pupils, the rats were then placed on the operating table of an ERG device (MAYO LS-100, Inazawa, Aichi, Japan), the ground electrode was held at the root of the tail of the rats, the electrode was recorded close to the cornea, and the dark-adapted ERG response was

measured at a light intensity of 3.0 cd*s/m^2. The amplitudes of a and b waves were recorded, and the data were analyzed using GraphPad Prism 6.

Immunofluorescence staining and terminal deoxynucleotidyl TUNEL assays

Immunofluorescence staining and terminal deoxynucleotidyl TUNEL assays were performed as previously reported [86]. The rats were sacrificed at the testing time, and the eyeballs were separated, fixed in 4% paraformaldehyde (PFA) at room temperature for 1.5 h, and then transferred to 30% sucrose at 4 °C overnight. The samples were immersed in Optimal Cutting Temperature (OCT) (Sakura FineTek, Torrance, CA, USA) to generate frozen tissue and cut into slices 10-μm thick on the sagittal plane. For the cells, we first fixed the slides in 4% PFA at 4 °C for 20 min, before incubating them with 0.3% Triton X-100 and 3% bovine serum albumin (BSA) at 37 °C for 30 min. The tissue sections and cell slides to be stained were soaked in 1% BSA + 0.1% Triton-diluted primary antibody and incubated at 4 °C overnight. Fluorophore-conjugated secondary antibodies diluted in PBS were then incubated at 37 °C for 1 h. For TUNEL staining (In Situ Cell Death Detection Kit, Roche, Basel, Switzerland), according to the manufacturer's instructions, buffers 1 and 2 were mixed in a ratio of 1:9, immersed in tissue or cells, and incubated at 37 °C for 2 h. Following incubation, the samples were incubated at room temperature in dimercaptophenylhydrazine solution (4′,6-diamidino-2-phenylindole, DAPI; Sigma) for 10 min. Visualization was achieved through confocal microscopy (Zeiss LSM 800 confocal microscope, ZEN Microsystems; ZEISS, Germany).

tRF and tiRNA sequencing

To assess the integrity of the total RNA samples, agarose gel electrophoresis was employed, while quantification of the samples was conducted using a NanoDrop ND-1000 instrument. The total RNA samples underwent pretreatment steps to eliminate certain RNA modifications that interfere with the construction of small RNA-seq libraries. These steps included deacylation of the 3'-aminoacyl (charged) group to convert it into 3'-OH for subsequent ligation with the 3'-adaptor, removal of 3'-cP (2',3'-cyclic phosphate) to 3'-OH for 3'-adaptor ligation, phosphorylation of the 5'-OH (hydroxyl group) to generate 5'-P for 5'-adaptor ligation, and demethylation of m1A and m3C to enable efficient reverse transcription. The pretreated total RNA from each sample was then utilized for the preparation of tRF and tiRNA-seq libraries, following a series of steps: (1) ligation of the 3'-adapter, (2) ligation of the 5'-adapter, (3) cDNA synthesis, (4) PCR amplification, and (5) selection of PCR amplified fragments with a size range of approximately 134–160 bp, which corresponds to small RNA molecules of approximately 14–40 nt. The final libraries were quantified using an Agilent 2100 Bioanalyzer and subsequently pooled in equal proportions based on the quantification results, before being subjected to sequencing. The sequencing type was 50-bp single RNA. The assessment of sequencing quality control for each sample involved utilizing a quality (Q) score map. Samples with Q scores higher than 30(> 99.9% correct) were categorized as high-quality data.

Analysis of microglia

The Zeiss confocal imaging system was used to capture images of the same relative position of three groups of retinal sections. After processing the maximum intensity projections (MIPs), the image was transferred to Photoshop software (21.2.2) for grid system analysis. We counted the number of grid cross points for each cell to determine the morphology of the microglial cells in the sections. The numbers of $Iba1^+$, $CD86^+$ $Iba1^+$, and $CD206^+$ $Iba1^+$cells were quantitatively analyzed by cell counts in retinal sections.

Real-time quantitative polymerase chain reaction (RT-qPCR)

As previously reported, we followed the steps for PCR testing [1, 52]. The primer sequence used in our experiment was provided by Sangon Biotech (Shanghai, China), as shown in Table 1. First, total RNA was extracted from the sample with 1 mL of TRIzol™ (Sigma-Aldrich, St. Louis, MO, USA), 500 μL of isopropanol, 200 μL of chloroform, and 1 mL of 75% ethyl alcohol. The purity and concentration of RNA were then measured using

Table 1 List of primers

Name	Forward primer	Reverse primer
Rat		
β-Actin	*CCCCATTGAACACGGCATTGTCA*	*ACCCTCATAGATGGGCACAGTGT*
IL-1β	*TGTGGCAGCTACCTATGTCT*	*GGGAACATCACACACTAGCA*
TNF-α	*CTCAAGCCCTGGTATGAGCC*	*GGCTGGGTAGAGAACGGATG*
IL-6	*CTGGATATAACCAGGAAA*	*GTTGGGGTAGGAAGGACT*
iNOS	*ATCCCGAAACGCTACACT*	*ATCCACAACTCGCTCCAA*
Src	*TGGACAGTGGCGGATTCTAC*	*TTCTCATGCCTCAGTTTCTTCAT*
Mouse		
β-Actin	*TGAGCTGCGTTTTACACCCT*	*TTTGGGGGATGTTTGCTCCA*
IL-1β	*CCTGCAGCTGGAGAGTGTGGAT*	*TGTGCTCTGCTTGTGAGGTGCT*
TNF-α	*AGCCCACGTCGTAGCAAACCAC*	*AGGTACAACCCATCGGCTGGCA*
IL-6	*TAGTCCTTCCTACCCCAATTTCC*	*TTGGTCCTTAGCCACTCCTTC*
iNOS	*AAGTCCAGCCGCACCACCCT*	*GACAATCCACAACTCGCTCC*
Src	*CACATCCAAGCCTCAGACCC*	*CTTCCGACACCACAGCATACA*

a spectrophotometric instrument (Thermo Fisher). Reverse transcription was performed using the Prime Script RT Reagent Kit (Takara, Tokyo, Japan) according to the kit instructions, and qPCR was performed using SYBR Green qPCR Mix (Takara Bio Inc., Japan) with a CFX96 Real-Time PCR System (Bio-rad, Hercules, CA, USA). The PCR conditions were as follows: 30 s at 95 °C, 41 cycles of 5 s at 95 °C and 30 s at 60 °C, followed by plate reading, and then 10 s at 95 °C, followed by melting curve analysis (65–95 °C in increments of 0.5 °C per 5 s).

Statistical analysis

Data are reported as the mean ± SEM. Student's two-tailed t-test was employed for our experiments. All results were replicated more than three times, and representative results are presented. *P*-values < 0.05 indicate significant differences. Statistical graphs were analyzed and drawn using GraphPad Prism 6.

Supplementary Information

The online version contains supplementary material available at https://doi.org/10.1186/s12964-024-01920-3.

Supplementary Material 1.

Acknowledgements

Not applicable.

Authors' contributions

A LD. designed and operated most of the experiments, wrote the main manuscript text, and integrated the figures. Xu HW., Xie J. and Qu LH. designed the experiments, checked, and revised the manuscript text and figures. Xu HW., and Qu LH. provided funding support. Ge LL. performed PCR tests. He JC., Gong H., Liang QL. checked and revised the manuscript text. Chen SY., Huang XN., Gao H. and You TJ. assisted with some of the experiments. All authors reviewed and approved the final manuscript.

Funding

This work was supported by grants from the National Natural Science Foundation of China (81800874, 31930068), the National Key Research and Development Program of China (Grant No. 2021YFA1101203), and the Medical Science and Technology Research Fund of Guangdong Province(A2021019).

Data availability

No datasets were generated or analysed during the current study.

Declarations

Ethics approval and consent to participate

The authors declare that they have consented to the scientific content and authorship of this study. This study was approved by the Institutional Animal Care and Use Committee of Army Medical University, Chongqing, China. All animal trials were approved by the Army Medical University Institutional Review Board, and all trials met guidelines. The production certificate number for our laboratory animal is SCXK-PLA-20120011, and the occupancy permit number is SYXK-PLA-20120031. All procedures in this study were approved.

Competing interests

The authors declare no competing interests.

Author details

[1]Southwest Hospital/Southwest Eye Hospital, Third Military Medical University (Army Medical University, Chongqing 400038, China. [2]Key Lab of Visual Damage and Regeneration & Restoration of Chongqing, Chongqing 400038, China. [3]Department of Ophthalmology, The 74th Army Group Hospital, Guangzhou 510318, China. [4]Shigatse Branch of Xinqiao Hospital, 953th Hospital, Army Medical University (Third Military Medical University), Shigatse 857000, China. [5]Department of Military Cognitive Psychology, School of Psychology, Army Medical University, Chongqing 400038, China. [6]Department of Clinical Laboratory Medicine, First Affiliated Hospital, Third Military Medical University (Army Medical University), Chongqing, China.

Received: 22 July 2024 Accepted: 1 November 2024
Published online: 13 November 2024

References

1. Zou T, Gao L, Zeng Y, Li Q, Li Y, Chen S, Hu X, Chen X, Fu C, Xu H, et al. Organoid-derived C-Kit(+)/SSEA4(-) human retinal progenitor cells promote a protective retinal microenvironment during transplantation in rodents. Nat Commun. 2019;10(1):1205. https://doi.org/10.1038/s41467-019-08961-0.
2. Cone AS, Yuan X, Sun L, Duke LC, Vreones MP, Carrier AN, Kenyon SM, Carver SR, Benthem SD, Stimmell AC, et al. Mesenchymal stem cell-derived extracellular vesicles ameliorate Alzheimer's disease-like phenotypes in a preclinical mouse model. Theranostics. 2021;11(17):8129–42. https://doi.org/10.7150/thno.62069.
3. Song N, Scholtemeijer M, Shah K. Mesenchymal stem cell immunomodulation: mechanisms and therapeutic potential. Trends Pharmacol Sci. 2020;41(9):653–64. https://doi.org/10.1016/j.tips.2020.06.009.
4. Jiang W, Xu J. Immune modulation by mesenchymal stem cells. Cell Prolif. 2020;53(1): e12712. https://doi.org/10.1111/cpr.12712.
5. Volkman R, Offen D. Concise review: mesenchymal stem cells in neurodegenerative diseases. Stem Cells. 2017;35(8):1867–80. https://doi.org/10.1002/stem.2651.
6. Alvites R, Branquinho M, Sousa AC, Lopes B, Sousa P, Maurício AC. Mesenchymal stem/stromal cells and their paracrine activity-immunomodulation mechanisms and how to influence the therapeutic potential. Pharmaceutics. 2022;14(2): 381. https://doi.org/10.3390/pharmaceutics14020381.
7. Xunian Z, Kalluri R. Biology and therapeutic potential of mesenchymal stem cell-derived exosomes. Cancer Sci. 2020;111(9):3100–10. https://doi.org/10.1111/cas.14563.
8. Ranganath SH, Levy O, Inamdar MS, Karp JM. Harnessing the mesenchymal stem cell secretome for the treatment of cardiovascular disease. Cell Stem Cell. 2012;10(3):244–58.
9. Yu D, Li Y, Wang M, Gu J, Xu W, Cai H, Fang X, Zhang X. Exosomes as a new frontier of cancer liquid biopsy. Mol Cancer. 2022;21(1):56. https://doi.org/10.1016/j.stem.2012.02.005.
10. Shen Z, Huang W, Liu J, Tian J, Wang S, Rui K. Effects of mesenchymal stem cell-derived exosomes on autoimmune diseases. Front Immunol. 2021;12:749192. https://doi.org/10.3389/fimmu.2021.749192.m.
11. Li Z, Liu F, He X, Yang X, Shan F, Feng J. Exosomes derived from mesenchymal stem cells attenuate inflammation and demyelination of the central nervous system in EAE rats by regulating the polarization of microglia. Int Immunopharmacol. 2019;67:268–80. https://doi.org/10.1016/j.intimp.2018.12.001.
12. Bai L, Shao H, Wang H, Zhang Z, Su C, Dong L, Yu B, Chen X, Li X, Zhang X. Effects of mesenchymal stem cell-derived exosomes on experimental autoimmune uveitis. Sci Rep. 2017;7(1):4323. https://doi.org/10.1038/s41598-017-04559-y.
13. Shigemoto-Kuroda T, Oh JY, Kim DK, Jeong HJ, Park SY, Lee HJ, Park JW, Kim TW, An SY, Prockop DJ, et al. MSC-derived extracellular vesicles attenuate immune responses in two autoimmune murine models: type 1 diabetes and uveoretinitis. Stem Cell Rep. 2017;8(5):1214–25. https://doi.org/10.1016/j.stemcr.2017.04.008.
14. Mathew B, Ravindran S, Liu X, Torres L, Chennakesavalu M, Huang CC, Feng L, Zelka R, Lopez J, Sharma M, et al. Mesenchymal stem cell-derived extracellular vesicles and retinal ischemia-reperfusion. Biomaterials. 2019;197:146–60. https://doi.org/10.1016/j.biomaterials.2019.01.016.

15. Liu S, Fan M, Xu JX, Yang LJ, Qi CC, Xia QR, Ge JF. Exosomes derived from bone-marrow mesenchymal stem cells alleviate cognitive decline in AD-like mice by improving BDNF-related neuropathology. J Neuroinflammation. 2022;19(1):35. https://doi.org/.
16. Joo HS, Suh JH, Lee HJ, Bang ES, Lee JM. Current knowledge and future perspectives on mesenchymal stem cell-derived exosomes as a new therapeutic agent. Int J Mol Sci. 2020;21(3):727. https://doi.org/.
17. Yu Z, Wen Y, Jiang N, Li Z, Guan J, Zhang Y, Deng C, Zhao L, Zheng SG, Zhu Y, et al. TNF-alpha stimulation enhances the neuroprotective effects of gingival MSCs derived exosomes in retinal ischemia-reperfusion injury via the MEG3/miR-21a-5p axis. Biomaterials. 2022;284121484. https://doi.org/10.1186/s12974-022-02393-2.
18. Riazifar M, Mohammadi MR, Pone EJ, Yeri A, Lässer C, Segaliny AI, McIntyre LL, Shelke GV, Hutchins E, Hamamoto A, et al. Stem cell-derived exosomes as nanotherapeutics for autoimmune and neurodegenerative disorders. ACS Nano. 2019;13(6):6670–88. https://doi.org/10.1021/acsnano.9b01004.
19. Newton F, Megaw R. Mechanisms of photoreceptor death in retinitis pigmentosa. Genes (Basel). 2020;11(10): 1120. https://doi.org/10.3390/genes11101120.
20. Verbakel SK, van Huet RAC, Boon CJF, den Hollander AI, Collin RWJ, Klaver CCW, Hoyng CB, Roepman R, Klevering BJ. Non-syndromic retinitis pigmentosa. Prog Retin Eye Res. 2018;66:157–86. https://doi.org/10.1016/j.preteyeres.2018.03.005.
21. Zhai W, Gao L, Qu L, Li Y, Zeng Y, Li Q, Xu H, Yin ZQ. Combined transplantation of olfactory ensheathing cells with rat neural stem cells enhanced the therapeutic effect in the retina of RCS rats. Front Cell Neurosci. 2020;14: 52. https://doi.org/10.3389/fncel.2020.00052.
22. Debbi L, Guo S, Safina D, Levenberg S. Boosting extracellular vesicle secretion. Biotechnol Adv. 2022. https://doi.org/10.1016/j.biotechadv.2022.107983.
23. YGuo S, Debbi L, Zohar B, Samuel R, Arzi RS, Fried AI, Carmon T, Shevach D, Redenski I, Schlachet I, et al. Stimulating extracellular vesicles production from engineered tissues by mechanical forces. Nano Lett. 2021;21(6):2497–504. https://doi.org/10.1021/acs.nanolett.0c04834.
24. Jafari D, Malih S, Eini M, Jafari R, Gholipourmalekabadi M, Sadeghizadeh M, Samadikuchaksaraei A. Improvement, scaling-up, and downstream analysis of exosome production. Crit Rev Biotechnol. 2020;40(8):1098–112. https://doi.org/10.1080/07388551.2020.1805406.
25. Logozzi M, Mizzoni D, Angelini DF, Di Raimo R, Falchi M, Battistini L, Fais S. Microenvironmental pH and exosome levels interplay in human cancer cell lines of different histotypes. Cancers (Basel). 2018;10(10):370. https://doi.org/10.3390/cancers10100370.
26. Park UC, Park SS, Kim BH, Park SW, Kim YJ, Cary W, Anderson JD, Nolta JA, Yu HG. Subretinal versus intravitreal administration of human CD34 + bone marrow-derived stem cells in a rat model of inherited retinal degeneration. Ann Transl Med. 2021;9(15):1275. https://doi.org/10.21037/atm-20-4662.
27. Yang R, Huang H, Cui S, Zhou Y, Zhang T, Zhou Y. IFN-gamma promoted exosomes from mesenchymal stem cells to attenuate colitis via miR-125a and miR-125b. Cell Death Dis. 2020;11(7):603. https://doi.org/10.1038/s41419-020-02788-0.
28. YZhang J, Lu Y, Mao Y, Yu Y, Wu T, Zhao W, Zhu Y, Zhao P, Zhang F. IFN-gamma enhances the efficacy of mesenchymal stromal cell-derived exosomes via miR-21 in myocardial infarction rats. Stem Cell Res Ther. 2022;13(1):333. https://doi.org/10.1186/s13287-022-02984-z.
29. Yoon J, Lee SK, Park A, Lee J, Jung I, Song KB, Choi EJ, Kim S, Yu J. Exosome from IFN-gamma-primed induced pluripotent stem cell-derived mesenchymal stem cells improved skin inflammation and barrier function. Int J Mol Sci. 2023;24(14):11635. https://doi.org/10.3390/ijms241411635.
30. Lu W, Du X, Zou S, Fang Q, Wu M, Li H, Shi B. IFN-gamma enhances the therapeutic efficacy of MSCs-derived exosome via mir-126-3p in diabetic wound healing by targeting SPRED1. J Diabetes. 2024;16(1): e13465. https://doi.org/10.1111/1753-0407.13465.
31. Wang C, Yang Y, Jiang C, Xi C, Yin Y, Wu H, Qian C. Exosomes derived from hucMSCs primed with IFN-gamma suppress the NF-kappaB signal pathway in LPS-induced ALI by modulating the miR-199b-5p/AFTPH Axis. Cell Biochem Biophys. 2024. https://doi.org/10.1007/s12013-023-01208-2.
32. Zhang G, Zhu Z, Wang H, Yu Y, Chen W, Waqas A, Wang Y, Chen L. Exosomes derived from human neural stem cells stimulated by interferon gamma improve therapeutic ability in ischemic stroke model. J Adv Res. 2020;24:435–45. https://doi.org/10.1016/j.jare.2020.05.017.
33. Bulati M, Miceli V, Gallo A, Amico G, Carcione C, Pampalone M, Conaldi PG. The immunomodulatory properties of the human amnion-derived mesenchymal stromal/stem cells are induced by INF-gamma produced by activated lymphomonocytes and are mediated by cell-to-cell contact and soluble factors. Front Immunol. 2020;11:54. https://doi.org/10.3389/fimmu.2020.00054.
34. Hu Y, Cai A, Xu J, Feng W, Wu A, Liu R, Cai W, Chen L, Wang F. An emerging role of the 5′ termini of mature tRNAs in human diseases: current situation and prospects. Biochim Biophys Acta Mol Basis Dis. 2022;1868(2):166314. https://doi.org/10.1016/j.bbadis.2021.166314.
35. Chiou NT, Kageyama R, Ansel KM. Selective export into extracellular vesicles and function of tRNA fragments during T cell activation. Cell Rep. 2018;25(12):3356–3370.e4. https://doi.org/10.1016/j.celrep.2018.11.073.
36. Gámbaro F, Li Calzi M, Fagúndez P, Costa B, Greif G, Mallick E, Lyons S, Ivanov P, Witwer K, Cayota A, et al. Stable tRNA halves can be sorted into extracellular vesicles and delivered to recipient cells in a concentration-dependent manner. RNA Biol. 2020;17(8):1168–82. https://doi.org/10.1080/15476286.2019.1708548.
37. Telonis AG, Loher P, Honda S, Jing Y, Palazzo J, Kirino Y, Rigoutsos I. Dissecting tRNA-derived fragment complexities using personalized transcriptomes reveals novel fragment classes and unexpected dependencies. Oncotarget. 2015;6(28):24797–822. https://doi.org/10.18632/oncotarget.4695.
38. Olvedy M, Scaravilli M, Hoogstrate Y, Visakorpi T, Jenster G, Martens-Uzunova ES. A comprehensive repertoire of tRNA-derived fragments in prostate cancer. Oncotarget. 2016;7(17):24766–77. https://doi.org/10.18632/oncotarget.8293.
39. Zong T, Yang Y, Zhao H, Li L, Liu M, Fu X, Tang G, Zhou H, Aung LHH, Li P, et al. tsRNAs: novel small molecules from cell function and regulatory mechanism to therapeutic targets. Cell Prolif. 2021;54(3): e12977. https://doi.org/10.1111/cpr.12977.
40. Shi J, Zhang Y, Zhou T, Chen Q. tsRNAs: the Swiss army knife for translational regulation. Trends Biochem Sci. 2019;44(3):185–9. https://doi.org/10.1016/j.tibs.2018.09.007.
41. Drino A, Oberbauer V, Troger C, Janisiw E, Anrather D, Hartl M, Kaiser S, Kellner S, Schaefer MR. Production and purification of endogenously modified tRNA-derived small RNAs. RNA Biol. 2020;17(8):1104–15. https://doi.org/10.1080/15476286.2020.1733798.
42. Xie Y, Yao L, Yu X, Ruan Y, Li Z, Guo J. Action mechanisms and research methods of tRNA-derived small RNAs. Signal Transduct Target Ther. 2020;5(1):109. https://doi.org/10.1038/s41392-020-00217-4.
43. Fang S, He T, Jiang J, Li Y, Chen P. Osteogenic effect of tsRNA-10277-Loaded exosome derived from bone mesenchymal stem cells on steroid-induced osteonecrosis of the femoral head. Drug Des Devel Ther. 2020;14:4579–91. https://doi.org/10.2147/DDDT.S258024.
44. Yang W, Gao K, Qian Y, Huang Y, Xiang Q, Chen C, Chen Q, Wang Y, Fang F, He Q, et al. A novel tRNA-derived fragment AS-tDR-007333 promotes the malignancy of NSCLC via the HSPB1/MED29 and ELK4/MED29 axes. J Hematol Oncol. 2022;15(1):53. https://doi.org/10.1186/s13045-022-01270-y.
45. Kumar P, Kuscu C, Dutta A. Biogenesis and function of transfer RNA-related fragments (tRFs). Trends Biochem Sci. 2016;41(8):679–89. https://doi.org/10.1016/j.tibs.2016.05.004.
46. Keam SP, Sobala A, Ten Have S, Hutvagner G. tRNA-derived RNA fragments associate with human multisynthetase complex (MSC) and modulate ribosomal protein translation. J Proteome Res. 2017;16(2):413–20. https://doi.org/10.1021/acs.jproteome.6b00267.
47. Wen JT, Huang ZH, Li QH, Chen X, Qin HL, Zhao Y. Research progress on the tsRNA classification, function, and application in gynecological malignant tumors. Cell Death Discov. 2021;7(1):388. https://doi.org/10.1038/s41420-021-00789-2.
48. Chen Q, Yan M, Cao Z, Li X, Zhang Y, Shi J, Feng GH, Peng H, Zhang X, Zhang Y, et al. Sperm tsRNAs contribute to intergenerational inheritance of an acquired metabolic disorder. Science. 2016;351(6271):397–400. https://doi.org/10.1126/science.aad7977.

49. Tkach M, Thery C. Communication by extracellular vesicles: where we are and where we need to go. Cell. 2016;164(6):1226–32. https://doi.org/10.1016/j.cell.2016.01.043.
50. Dou R, Zhang X, Xu X, Wang P, Yan B. Mesenchymal stem cell exosomal tsRNA-21109 alleviate systemic lupus erythematosus by inhibiting macrophage M1 polarization. Mol Immunol. 2021;139:106–14. https://doi.org/10.1016/j.molimm.2021.08.015.
51. Zhu L, Li J, Gong Y, Wu Q, Tan S, Sun D, Xu X, Zuo Y, Zhao Y, Wei YQ, et al. Exosomal tRNA-derived small RNA as a promising biomarker for cancer diagnosis. Mol Cancer. 2019;18(1):74. https://doi.org/10.1186/s12943-019-1000-8.
52. Bian B, Zhao C, He X, Gong Y, Ren C, Ge L, Zeng Y, Li Q, Chen M, Weng C, et al. Exosomes derived from neural progenitor cells preserve photoreceptors during retinal degeneration by inactivating microglia. J Extracell Vesicles. 2020;9(1): 1748931. https://doi.org/10.1080/20013078.2020.1748931.
53. He J, Fu Y, Ge L, Dai J, Fang Y, Li Y, Gu X, Tao Z, Zou T, Li M, et al. Disease-associated microglial activation prevents photoreceptor degeneration by suppressing the accumulation of cell debris and neutrophils in degenerating rat retinas. Theranostics. 2022;12(6):2687–706. https://doi.org/10.7150/thno.67954.
54. Martinez-Vacas A, Di Pierdomenico J, Gallego-Ortega A, Valiente-Soriano FJ, Vidal-Sanz M, Picaud S, Villegas-Pérez MP, García-Ayuso D. Systemic taurine treatment affords functional and morphological neuroprotection of photoreceptors and restores retinal pigment epithelium function in RCS rats. Redox Biol. 2022;57: 102506. https://doi.org/10.1016/j.redox.2022.102506.
55. Wang SK, Cepko CL. Targeting microglia to treat degenerative eye diseases. Front Immunol. 2022. https://doi.org/10.3389/fimmu.2022.843558.
56. Murakami Y, Nakabeppu Y, Sonoda KH. Oxidative stress and microglial response in retinitis pigmentosa. Int J Mol Sci. 2020;21(19):7170. https://doi.org/10.3390/ijms21197170.
57. Wiacek MP, Goslawski W, Grabowicz A, Sobuś A, Kawa MP, Baumert B, Paczkowska E, Milczarek S, Osękowska B, Safranow K, et al. Long-term effects of adjuvant intravitreal treatment with autologous bone marrow-derived lineage-negative cells in retinitis pigmentosa. Stem Cells Int. 2021. https://doi.org/10.1155/2021/6631921.
58. Ding SSL, Subbiah SK, Khan MSA, Farhana A, Mok PL. Empowering mesenchymal stem cells for ocular degenerative disorders. Int J Mol Sci. 2019;20(7): 1784. https://doi.org/10.3390/ijms20071784.
59. Duijvestein M, Wildenberg ME, Welling MM, Hennink S, Molendijk I, van Zuylen VL, Bosse T, Vos AC, de Jonge-Muller ES, Roelofs H, et al. Pretreatment with interferon-gamma enhances the therapeutic activity of mesenchymal stromal cells in animal models of colitis. Stem Cells. 2011;29(10):1549–58. https://doi.org/10.1002/stem698.
60. Zhang Q, Fu L, Liang Y, Guo Z, Wang L, Ma C, Wang H. Exosomes originating from MSCs stimulated with TGF-beta and IFN-gamma promote Treg differentiation. J Cell Physiol. 2018;233(9):6832–40. https://doi.org/10.1002/jcp.26436.
61. Lee YS, Shibata Y, Malhotra A, Dutta A. A novel class of small RNAs: tRNA-derived RNA fragments (tRFs). Genes Dev. 2009;23(22):2639–49. https://doi.org/10.1101/gad1837609.
62. Lue H, Kapurniotu A, Fingerle-Rowson G, Roger T, Leng L, Thiele M, Calandra T, Bucala R, Bernhagen J. Rapid and transient activation of the ERK MAPK signalling pathway by macrophage migration inhibitory factor (MIF) and dependence on JAB1/CSN5 and Src kinase activity. Cell Signal. 2006;18(5):688–703. https://doi.org/10.1016/j.cellsig.2005.06.013.
63. Dhawan G, Combs CK. Inhibition of src kinase activity attenuates amyloid associated microgliosis in a murine model of Alzheimer's disease. J Neuroinflammation. 2012;9:117. https://doi.org/10.1186/1742-2094-9-117.
64. Zhang L, Liu J, Hou Y. Classification, function, and advances in tsRNA in non-neoplastic diseases. Cell Death Dis. 2023;14(11):748. https://doi.org/10.1038/s41419-023-06250-9.
65. Dou S, Wang Y, Lu JM, tsRNAs. Biogenesis, evolution and regulatory functions. Noncoding RNA. 2019;5(1): 18. https://doi.org/10.3390/ncrna5010018.
66. Gebetsberger J, Wyss L, Mleczko AM, Reuther J. Polacek N.A tRNA-derived fragment competes with mRNA for ribosome binding and regulates translation during stress. RNA Biol. 2017;14(10):1364–73. https://doi.org/10.1080/15476286.2016.1257470.
67. Torres AG. Enjoy the silence: nearly half of human tRNA genes are silent. Bioinform Biol Insights. 2019;13:1177932219868454. https://doi.org/10.1177/1177932219868454.
68. Lyons SM, Gudanis D, Coyne SM, Gdaniec Z, Ivanov P. Identification of functional tetramolecular RNA G-quadruplexes derived from transfer RNAs. Nat Commun. 2017;8:1127. https://doi.org/10.1038/s41467-017-01278-w.
69. Liang Y, Ji D, Ying X, Ma R, Ji W. tsRNA modifications: an emerging layer of biological regulation in disease. J Adv Res. 2024;S2090–1232(24):00401–6. https://doi.org/10.1016/j.jare.2024.09.010.
70. Kim HK, Fuchs G, Wang S, Wei W, Zhang Y, Park H, Roy-Chaudhuri B, Li P, Xu J, Chu K, et al. A transfer-RNA-derived small RNA regulates ribosome biogenesis. Nature. 2017;552(7683):57–62. https://doi.org/10.1038/nature25005.
71. Kuhle B, Chen Q, Schimmel P. tRNA renovatio: rebirth through fragmentation. Mol Cell. 2023;83(22):3953–71. https://doi.org/10.1016/j.molcel.2023.09.016.
72. Wendimu MY, Hooks SB. Microglia phenotypes in aging and neurodegenerative diseases. Cells. 2022;11(13): 2091. https://doi.org/10.3390/cells11132091.
73. He J, Zhao C, Dai J, Weng CH, Bian BSJ, Gong Y, Ge L, Fang Y, Liu H, Xu H, et al. Microglia mediate synaptic material clearance at the early stage of rats with retinitis pigmentosa. Front Immunol. 2019. https://doi.org/10.3389/fimmu.2019.00912.
74. Xu H, Chen M. Immune response in retinal degenerative diseases - time to rethink? Prog Neurobiol. 2022;219: 102350. https://doi.org/10.1016/j.pneurobio.2022.102350.
75. Yu A, Zhang T, Duan H, Pan Y, Zhang X, Yang G, Wang J, Deng Y, Yang Z. MiR-124 contributes to M2 polarization of microglia and confers brain inflammatory protection via the C/EBP-alpha pathway in intracerebral hemorrhage. Immunol Lett. 2017;182:1–11. https://doi.org/10.1016/j.imlet.2016.12.003.
76. Socodato R, Portugal CC, Domith I, Oliveira NA, Coreixas VS, Loiola EC, Martins T, Santiago AR, Paes-de-Carvalho R, Ambrósio AF, et al. c-Src function is necessary and sufficient for triggering microglial cell activation. Glia. 2015;63(3):497–511. https://doi.org/10.1002/glia.22767.
77. Palanisamy CP, Pei J, Alugoju P, Anthikapalli NVA, Jayaraman S, Veeraraghavan VP, Gopathy S, Roy JR, Janaki CS, Thalamati D, et al. New strategies of neurodegenerative disease treatment with extracellular vesicles (EVs) derived from mesenchymal stem cells (MSCs). Theranostics. 2023;13(12):4138–65. https://doi.org/10.7150/thno.83066.
78. Joo HS, Suh JH, Lee HJ, Bang ES, Lee JM. Current knowledge and future perspectives on mesenchymal stem cell-derived exosomes as a new therapeutic agent. Int J Mol Sci. 2020;21(3): 727. https://doi.org/10.3390/ijms21030727.
79. Rozier P, Maumus M, Maria ATJ, Toupet K, Jorgensen C, Guilpain P, Noël D. Lung fibrosis is improved by extracellular vesicles from IFNγ-primed mesenchymal stromal cells in murine systemic sclerosis. Cells. 2021;10(10):2727. https://doi.org/10.3390/cells10102727.
80. Tan YL, Al-Masawa ME, Eng SP, Shafiee MN, Law JX, Ng MH. Therapeutic efficacy of interferon-Gamma and hypoxia-primed mesenchymal stromal cells and their extracellular vesicles: underlying mechanisms and potentials in clinical translation. Biomedicines. 2024;12(6): 1369. https://doi.org/10.3390/biomedicines12061369.
81. Jiang Z, Wang H, Yu K, Feng Y, Wang Y, Huang T, Lai K, Xi Y, Yang G. Light-controlled BMSC sheet-implant complexes with improved osteogenesis via an LRP5/beta-Catenin/Runx2 regulatory loop. ACS Appl Mater Interfaces. 2017;9(40):34674–86. https://doi.org/10.1021/acsami.7b10184.
82. Deng CL, Hu CB, Ling ST, Zhao N, Bao LH, Zhou F, Xiong YC, Chen T, Sui BD, Yu XR, et al. Photoreceptor protection by mesenchymal stem cell transplantation identifies exosomal MiR-21 as a therapeutic for retinal degeneration. Cell Death Differ. 2021;28(3):1041–61. https://doi.org/10.1038/s41418-020-00636-4.
83. Chu DT, Phuong TNT, Tien NLB, Tran DK, Thanh VV, Quang TL, Truong DT, Pham VH, Ngoc VTN, Chu-Dinh T, et al. An update on the progress of isolation, culture, storage, and clinical application of human bone marrow mesenchymal Stem/Stromal cells. Int J Mol Sci. 2020;21(3): 708. https://doi.org/10.3390/ijms21030708.
84. Hu Y, Zhang Y, Ni CY, Chen CY, Rao SS, Yin H, Huang J, Tan YJ, Wang ZX, Cao J, et al. Human umbilical cord mesenchymal stromal cells-derived extracellular vesicles exert potent bone protective effects

by CLEC11A-mediated regulation of bone metabolism. Theranostics. 2020;10(5):2293–308. https://doi.org/10.7150/thno.39238.
85. Lin Y, Zhang C, Xiang P, Shen J, Sun W, Yu H. Exosomes derived from HeLa cells break down vascular integrity by triggering endoplasmic reticulum stress in endothelial cells. J Extracell Vesicles. 2020;9(1):1722385. https://doi.org/10.1080/20013078.2020.1722385.
86. Zou AL, He T, Chen J, Sun X, Fan D, Xu X. Rescue of retinal degeneration in rd1 mice by intravitreally injected metformin. Front Mol Neurosci. 2019;12: 102. https://doi.org/10.3389/fnmol.2019.00102.
87. Oubaha M, Miloudi K, Dejda A, Guber V, Mawambo G, Germain MA, Bourdel G, Popovic N, Rezende FA, Kaufman RJ, et al. Senescence-associated secretory phenotype contributes to pathological angiogenesis in retinopathy. Sci Transl Med. 2016;8(362):362ra144.https://doi.org/10.1126/scitranslmedaaf9440.
88. Dai J, Fu Y, Zeng Y, Li S, Qin Yin Z. Improved retinal function in RCS rats after suppressing the over-activation of mGluR5. Sci Rep. 2017;7(1):3546. https://doi.org/10.1038/s41598-017-03702-z.

Publisher's Note